

FlexMS is a flexible framework for benchmarking deep learning-based mass spectrum prediction tools in metabolomics

Yunhua Zhong^{1†}, Yixuan Tang^{1,4†}, Yifan Li¹, Jie Yang^{1,3}, Pan Liu¹, Jun Xia^{1,2*}

^{1*}The Hong Kong University of Science and Technology (Guangzhou) .

²The Hong Kong University of Science and Technology .

³Fudan University .

⁴Jinan University .

*Corresponding author(s). E-mail(s): junxia@hkust-gz.edu.cn;

Contributing authors: yunhuazhong@hkust-gz.edu.cn; tangyixuan@stu2022.jnu.edu.cn;
yli994@connect.hkust-gz.edu.cn; yangjie23@m.fudan.edu.cn; panliu@hkust-gz.edu.cn;

[†]These authors contributed equally to this work.

Abstract

The identification and property prediction of chemical molecules is of central importance in the advancement of drug discovery and material science, where the tandem mass spectrometry technology gives valuable fragmentation cues in the form of mass-to-charge ratio peaks. However, the lack of experimental spectra hinders the attachment of each molecular identification, and thus urges the establishment of prediction approaches for computational models. Deep learning models appear promising for predicting molecular structure spectra, but overall assessment remains challenging as a result of the heterogeneity in methods and the lack of well-defined benchmarks. To address this, our contribution is the creation of benchmark framework FlexMS for constructing and evaluating diverse model architectures in mass spectrum prediction. With its easy-to-use flexibility, FlexMS supports the dynamic construction of numerous distinct combinations of model architectures, while assessing their performance on preprocessed public datasets using different metrics. In this paper, we provide insights into factors influencing performance, including the structural diversity of datasets, hyperparameters like learning rate and data sparsity, pretraining effects, metadata ablation settings and cross-domain transfer learning analysis. This provides practical guidance in choosing suitable models. Moreover, retrieval benchmarks simulate practical identification scenarios and score potential matches based on predicted spectra.

Keywords: Metabolomics, Mass Spectrum, Benchmark, Deep Learning

1 Introduction

Tandem mass spectra reveal fragmentation patterns that offer crucial structural insights into molecules. Mass spectrometry is an analytical technique that is used to identify and quantify chemicals in a mixture [1]. Molecules from the sample are ionized and then detected by a mass analyzer that records information about the mass-to-charge ratio of each ion in the form of a mass spectrum. Tandem mass spectrometry (MS/MS) is a variant of MS that includes a fragmentation step to isolate and break down charged precursor molecules into smaller fragments [2]. The mass spectrum is a distribution of the frequency or intensity of each type of ion, ordered by mass-to-charge ratio.

A common application of mass spectra is to determine the composition of a sample based on its mass spectrum. This typically involves searching the sample’s spectrum in a reference library [3]. However, since the number of molecules with experimentally determined mass spectra is far smaller than the total possible molecules, spectrum prediction methods can be used to generate synthetic datasets for mass spectral libraries [4]. Currently, commercial data sets contain about 10^4 different compounds and 10^6 spectra under different conditions, which is much smaller than the number of molecules in the human metabolism pathway [5].

Although unable to fully satisfy practical demands, the increasing availability of extensive public mass spectrometry datasets has enabled the development of data-driven models [6]. Consequently, machine learning and deep learning approaches are well-suited for spectrum prediction. In molecular representation for mass spectrum prediction, classical methods and traditional machine learning techniques—such as those using fixed-size molecular fingerprints—have laid the groundwork for more advanced deep learning models [7]. For instance, convolutional neural networks leverage SMILES-derived feature matrices for training [8], transformer-based models like ChemBERTa or MolBERT exploit sequential SMILES representations [9, 10], and graph neural networks (GNNs) are designed to process molecular graph structures [7]. These deep learning approaches extend and enhance the capabilities of their classical counterparts by capturing complex structural nuances. However, with the proliferation of such diverse models, establishing standardized benchmarks becomes essential to rigorously evaluate their effectiveness in mass spectrometry prediction tasks.

Despite rapid progress, the field still lacks standardized benchmarks to fairly assess models for MS/MS spectrum prediction. In practice, reported performance is confounded by many non-model factors—instrument settings like collision energies, ionization modes, preprocessing pipelines, data-splitting strategies that risk leakage, inconsistent MS/MS annotations, heterogeneous metrics, and limited or proprietary datasets. For example, ICEBERG [11] and SCARF [12] achieve strong results but are primarily trained on the commercial NIST20 dataset [13], and their models cannot be distributed due to licensing restrictions. ICEBERG also relies on the MAGMa algorithm [14] to annotate substructures in the breakage process to create a labeled data set, which may cost some hours before using them. Similarly, MassFormer [15] used a pretrained Graphormer model [16] as backbone and it may cost nearly an hour to run on a small demonstration data. These setting, time and data constraints hinder “out-of-the-box” exploration of mass spectra and make results difficult to compare across studies.

Furthermore, there is insufficient exploration of how different experimental and computational factors affect spectrum prediction, leaving practitioners with little guidance on model selection under specific conditions. Compounding these issues, existing toolchains are often complex to configure and reproduce across environments. To address these gaps and enable fair, actionable comparisons, we advocate building a process-aware, standardized benchmarking framework that (i) controls for acquisition heterogeneity, (ii) systematically quantifies the impact of key factors, and (iii) provides simple, reproducible tooling and protocols.

Building on this foundation, the primary task in prediction is to computationally model these dynamics. This has been achieved through several distinct frameworks, each offering unique advantages and limitations. **Fragmentation prediction** is grounded in the hypothesis that if one can systematically enumerate the possible bond cleavage events of a molecule, one can generate the set of possible fragment ions [17, 18]. **Binned prediction** offers a more tractable alternative by discretizing the continuous m/z space into fixed-width bins and treating spectrum prediction as a multi-label regression problem, where the model outputs intensity values for each predefined mass-to-charge (m/z) bin and effectively reconstructing the spectrum as a vector of binned intensities [19]. **Formula prediction** combines between the high-interpretability/low-speed of fragmentation models and the binned models with opposite feature. This approach represents a neuro-symbolic synthesis: it uses deep learning for speed and pattern recognition but enforces symbolic constraints to ensure validity [11].

We chose binned prediction primarily for its benchmarking simplicity and comparability. In this approach, the continuous m/z domain is discretized into fixed-width bins (typically 1 Da), transforming spectrum prediction into a multi-label regression problem where the model outputs intensity values for each bin, effectively reconstructing the spectrum as a vector of binned intensities. Other frameworks, such as fragmentation or formula prediction, may be constrained by their dependence on crafted heuristics for vocabulary generation and formula/structure annotation, potentially compromising their generalizability across diverse compound classes.

The paper is organized as follows. We first discussed the preliminaries for the prediction of the mass spectrum, including molecular representations, model architectures and computational frameworks. Subsequently, we provide the rationale behind this study and present our experiment schemes. To fully assess the effectiveness of molecular representation learning models, we also assembled a diverse set of datasets, including GNPS [20], MassBank [6], NPLIB1 [21], MassSpecGym [22], and the CASMI contest datasets [23]. Then the experimental results are presented and analyzed.

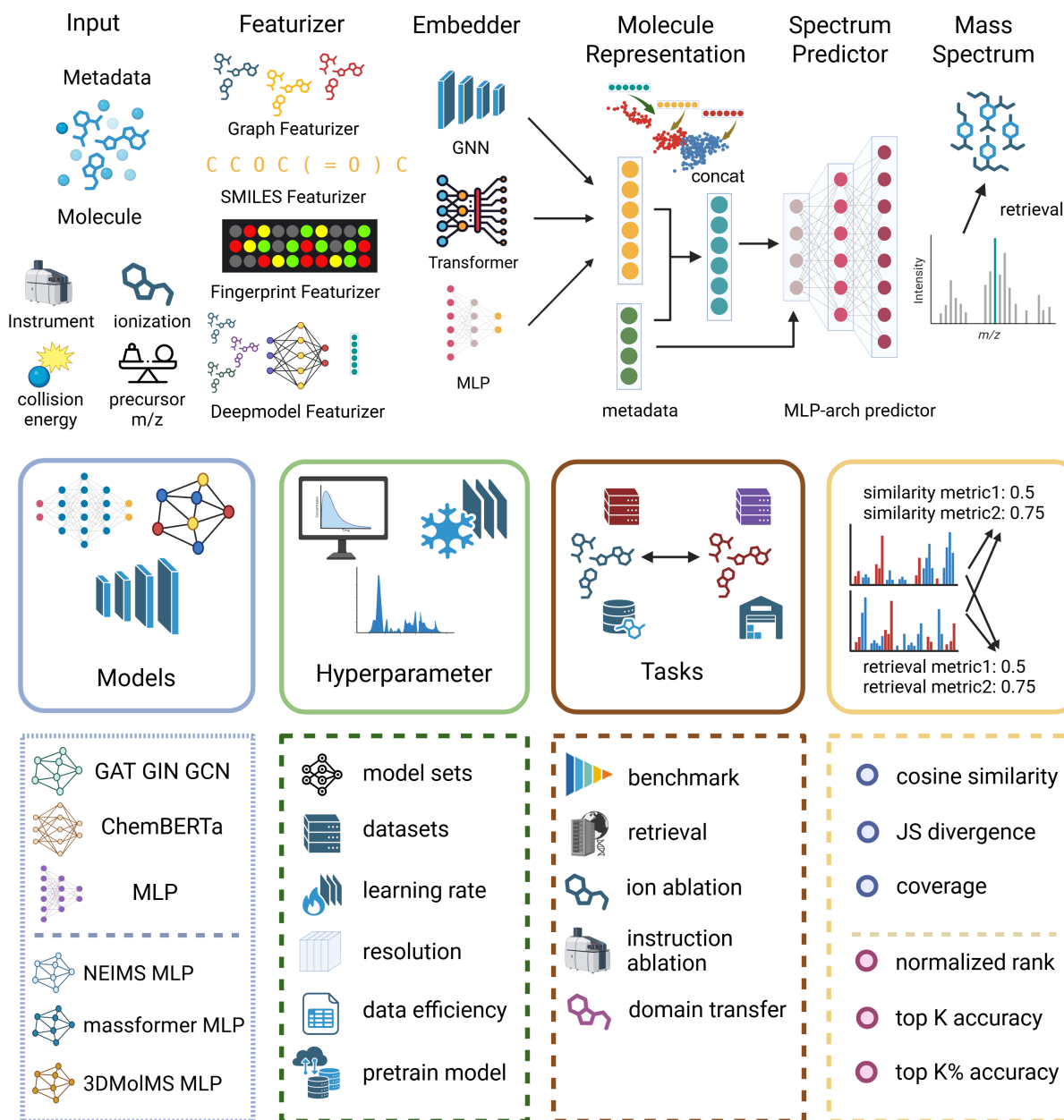


Fig. 1 Main components of FlexMS. We have developed a flexible framework, termed FlexMS, to systematically evaluate the performance of mass spectra prediction models. The framework takes molecules and associated metadata as inputs, employs various featurizers and embedders to generate molecular representations, and utilizes different multi-layer perceptron (MLP) architectures for spectrum prediction at specified bin resolutions. We assess the performance of various models, investigate the impact of different hyperparameters, and evaluate outcomes across diverse task scenarios. Comprehensive metrics are employed to quantify performance.

2 Results

2.1 Dataset Characterization in Mass Spectrum Prediction Benchmarks

2.1.1 Overview of Selected Datasets

In the rapidly evolving field of mass spectrum, the choice of datasets plays a pivotal role in ensuring robust generalization. We examined four prominent repositories: GNPS, MassBank, MIST-canopus, and MassSpecGym. GNPS is a collaborative platform for sharing tandem MS data from natural products [20]. MassBank provides reference mass spectra for diverse small molecules [6]. MIST-canopus offers tools for compound annotation from MS/MS spectra [21]. MassSpecGym is a benchmarking dataset for ML in mass spectrometry [22]. These datasets vary in scale and focus, with detailed assembly described in the subsequent sections.

2.1.2 Assessing Structural Diversity and Similarity in Statistical Insights

A key aspect of molecular datasets is the molecular structural diversity, which directly impacts the difficulty of prediction tasks [24]. We use multiple statistics to assess the diversity and similarity of dataset splits. We evaluated structural similarity using Tanimoto coefficients based on Morgan fingerprints [25], comparing different split types to simulate realistic training scenarios [26]. Scaffold splits enforce structural separation where novel scaffolds must be predicted without prior exposure, and random splits allow for potential overlap which may not fit real-world applicability [27].

Despite similar mean tanimoto similarity, the scaffold and random have different content of data leakage. To rigorously assess distributional shifts, we employed two-sample Kolmogorov-Smirnov tests [28] on Tanimoto similarity distributions. Scaffold splits consistently produce elevated KS statistics with highly significant p-values, confirming substantial distributional shifts that challenge model generalization. Random splits yield markedly lower statistics with minimal significance, indicating alignment suitable for initial prototyping. Predefined NLIB20 splits demonstrate random-like behavior, with MassSpecGym showing substantial shifts.

Scaffold overlap, the proportion of shared Murcko scaffolds [29] between splits, provides complementary structural redundancy metrics. Scaffold splits achieve zero overlap for GNPS and MassBank, enforcing strict separation. Random splits show moderate overlaps.

Train-Val	GNPS-S	GNPS-R	MB-S	MB-R	MSG	NPLIB1-0	NPLIB1-1	NPLIB1-2
Mean Tanimoto	0.1059	0.1056	0.0795	0.0875	0.1002	0.1032	0.1052	0.1055
KS-stat	0.0528	0.0024	0.0831	0.0044	0.0345	0.0188	0.0051	0.0039
Log KS-pval	-120.64	-0.03	-299.87	-0.53	-51.32	-14.97	-0.84	-0.36
Train-Test	GNPS-S	GNPS-R	MB-S	MB-R	MSG	NPLIB1-0	NPLIB1-1	NPLIB1-2
Mean Tanimoto	0.1045	0.1051	0.0788	0.0871	0.1005	0.1053	0.1052	0.1040
KS-stat	0.0326	0.0050	0.0794	0.0094	0.1002	0.0033	0.0020	0.0232
Log KS-pval	-45.74	-0.079	-274.18	-3.51	-61.88	-0.07	-0.01	-6.23

Table 1 Comparison of metrics across different datasets and splits. GNPS denotes the Global Natural Products Social molecular dataset, MB denotes MassBank, and MSG denotes MassSpecGym. The suffixes -R and -S indicate random and scaffold splits, respectively. NPLIB1-0, NPLIB1-1, and NPLIB1-2 correspond to predefined splits 0, 1, and 2 of the NLIB20 dataset.

2.1.3 Complementary Validation via Spectral Entropy Analysis

To provide independent validation from the spectral perspective, we further analyzed the distribution of spectral entropy across dataset splits. Spectral entropy [30], defined as $H = -\sum_i p_i \ln(p_i)$ where p_i represents the normalized peak intensity, quantifies the complexity of fragmentation patterns in mass spectra. While the Tanimoto-based analysis examines structural similarity at the molecular input level, spectral entropy captures differences in fragmentation behavior at the output level.

As shown in Table 2, the mean spectral entropy varies across datasets. GNPS, MassBank, and MassSpecGym exhibit similar entropy levels ($S \approx 1.6$ – 1.7), whereas NPLIB1 shows notably higher entropy ($S \approx 2.8$), reflecting the complex fragmentation patterns characteristic of natural products [30]. More importantly, scaffold splits exhibit substantially larger distributional shifts in spectral entropy compared to random splits. For GNPS, the KS statistic under scaffold split is 4.3 times higher than random split (0.011) with significant p-values, and MassBank shows a 7.1-fold increase in KS statistics for scaffold versus random splits similarly. Consistent with the Tanimoto analysis, scaffold-based partitioning isolates molecules with varying fragmentation complexities, imposing a stricter test of generalization for predictive models.

Train-Val	GNPS-S	GNPS-R	MB-S	MB-R	MSG	NPLIB1-0	NPLIB1-1	NPLIB1-2
Mean Entropy	1.7275	1.7169	1.6374	1.7027	1.7396	2.8494	2.8486	2.8326
KS-stat	0.0595	0.0054	0.1245	0.0163	0.0247	0.0340	0.0716	0.0586
Log KS-pval	-262.11	-1.66	-171.78	-2.13	-9.02	-0.44	-2.67	-1.76
Train-Test	GNPS-S	GNPS-R	MB-S	MB-R	MSG	NPLIB1-0	NPLIB1-1	NPLIB1-2
Mean Entropy	1.7275	1.7169	1.6374	1.7027	1.7396	2.8494	2.8486	2.8326
KS-stat	0.0492	0.0115	0.0995	0.0140	0.0137	0.0386	0.0332	0.0507
Log KS-pval	-172.84	-7.94	-88.19	-1.48	-2.33	-1.44	-1.01	-2.91

Table 2 Spectral entropy distribution analysis across dataset splits. Mean Entropy denotes the average Shannon entropy (in nats) of training set spectra. KS-stat and Log KS-pval report the Kolmogorov-Smirnov test statistics and \log_{10} -transformed p-values comparing entropy distributions between splits. Bold values indicate highly significant distributional shifts.

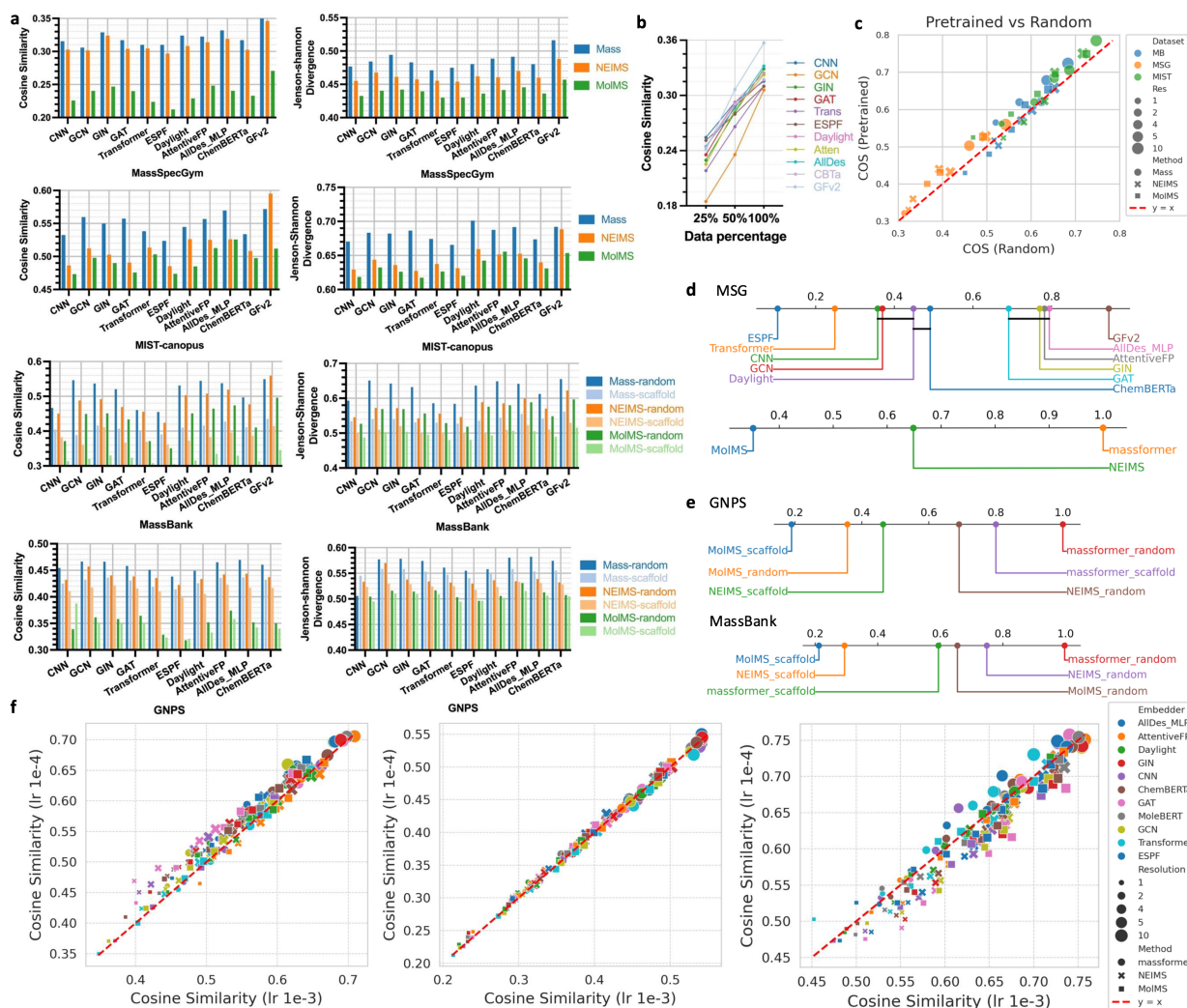


Fig. 2 Benchmark performance of different embedders and predictors. (a) The performance (cos similarity and Jensen-Shannon divergence) of different predictor-embedder combinations on four datasets. On GNPS and MassBank datasets, we compare the performance of random and scaffold splits. (b) The performance of different embedders on the MassSpecGym dataset when the amount of training data is limited (25%, 50% and 100%), using cosine similarity as the performance metric. (c) Paired performance scatter plot of pre-trained and random-initialized MoleBERT embedders on different datasets, resolutions and predictors. The color, shape and size of points represent different datasets, predictors and resolutions. (d)(e) Critical difference diagrams of different embedders and predictors on the MassSpecGym, GNPS and MassBank datasets, obtained by combining results across embedder-predictor pairs, resolutions and datasets, and applying the Wilcoxon-Holm test to detect pairwise significance. (f) Paired performance scatter plots of two learning rates on representative benchmark settings. The color, shape and size of points represent different embedders, predictors and resolutions.

2.2 Empirical study on embedder model and prediction model

The experimental results demonstrate varying performance across different embedder-predictor combinations on the MassSpecGym dataset [22], evaluated using cosine similarity and Jensen-Shannon divergence metrics.

Among the tested embedder approaches, GFv2 consistently achieved the highest performance across all predictor methods and resolutions, demonstrating its superior capability in molecular representation. Traditional graph-based methods like GIN [31] and GAT [32] showed competitive performance, while transformer-based approaches and CNN methods exhibited moderate results. The AllDescriptors-MLP approach also performed well. In Fig. 2a, we show the detailed performance. In Figs. 2d and 2e, we used critical difference diagrams [33] to illustrate the pairwise significance among different methods, based on the Wilcoxon-Holm test. The results indicate that simple MLP models based on all-descriptor fingerprints and attentive fingerprints also show comparable performance.

As shown in Fig. 2a, MassFormer [15] achieved the highest overall metrics across embedder combinations, followed by NEIMS [19], with MolMS [34] showing lower performance. Three MLP-based predictor architectures were evaluated for mass spectrometry spectrum prediction: MassFormer, NEIMS, and MolMS.

MassFormer uses a multi-layer perceptron with bidirectional prediction, gating mechanisms, and optional spectrum attention and output normalization. NEIMS employs a simpler linear output layer with optional reverse prediction and sigmoid activation, focusing on efficiency. MolMS features an encoder-decoder structure with convolutional layers for geometric feature extraction and residual blocks for added depth. Key differences include architectural complexity—MassFormer provides high flexibility, NEIMS emphasizes simplicity, and MolMS prioritizes convolutional processing—resulting in varied predictive performance.

The results in Fig. 2a indicate that certain embedder-predictor combinations work synergistically. For instance, the optimal combination of GFv2 embedder with MassFormer predictor achieved the best performance, while the same embedder with different predictors showed varying degrees of success. This highlights the importance of considering both components when designing mass spectrometry prediction models [35].

The substantial variation in performance across different method combinations (Figs. 2d and 2e) underscores the complexity of molecular representation learning for mass spectrometry prediction, as different architectural paradigms exhibit distinct synergistic relationships[36]. For instance, MolMS predictors demonstrate superior performance when paired with GNN-based embedders, as both components operate within the graph-theoretic framework that naturally captures molecular and spatial relationships [37]. Conversely, NEIMS shows enhanced effectiveness when combined with MLP-based embedders, reflecting its reliability on traditional architectures processing vectorized molecular representations. These findings demonstrate that effective mass spectrum prediction requires careful consideration of both molecular representation methods and prediction architectures, with certain combinations providing significantly better performance than others [7].

While GFv2 consistently delivers the best performance in our experiments, it comes with notable drawbacks in terms of model size and computational demands. As the largest embedder among those tested, GFv2 requires substantially more training time per batch and consumes significantly more GPU memory compared to other models. The computational overhead is particularly pronounced, with forward pass times being orders of magnitude slower than lightweight alternatives such as Transformer-based models, MBT, and simple architectures like CNN or GAT. Similarly, GPU memory consumption for GFv2 far exceeds that of other embedders, often requiring an order of magnitude more resources. Actually, training GFv2 on large dataset such as GNPS may cost several days even on largest GPU such as A100. The table 3 shows the time and GPU cost of different combinations.

These increased costs may be unacceptable in resource-constrained environments or when scaling to larger datasets. Furthermore, the performance gains offered by GFv2 are not always proportionate to these demands. In scenarios where marginal improvements in accuracy are not critical, more efficient alternatives like GIN, GAT or MLPs may provide a better trade-off between performance and resource efficiency, offering competitive results with dramatically lower computational requirements and faster training times.

Time(s)	CNN	GAT	GCN	GIN	Trans	ESPF	Attn*	DL*	AllDes*	MBT*	CBTa	GFv2
Mass*	0.532	0.823	0.656	0.658	0.270	0.395	0.690	0.394	0.351	0.259	3.493	123.5
NEIMS	0.471	0.594	0.581	0.564	0.212	0.324	0.527	0.355	0.346	0.228	3.432	121.9
MolMS	0.473	0.538	0.467	0.498	0.202	0.318	0.523	0.312	0.344	0.233	3.415	122.6
Peak(MB)	CNN	GAT	GCN	GIN	Trans	ESPF	Attn*	DL*	AllDes*	MBT*	CBTa	GFv2
Mass*	228.1	296.4	341.4	428.7	2882	538.1	1201	672.9	781.5	1295	982.2	24403
NEIMS	122.8	122.0	112.1	144.2	2554	135.2	746.7	165.2	209.7	719.8	476.7	23105
MolMS	271.9	272.5	264.0	299.7	2717	290.7	906.7	323.7	375.8	887.7	643.9	23587

Table 3 Computational efficiency comparison across model architectures. Time (seconds) and GPU memory (MB) per forward pass during training with batch size 512. Asterisks(*) indicate fingerprint-based and last two models are pretrained models. Column abbreviations: Trans=Transformer encoder, Atten=AttentiveFP-MLP, DL=Daylight-MLP, CBTa=ChemBERTa, AllDes=All-Descriptors-MLP, MBT=MoleBERT, GFv2=GraphormerV2. Row prefixes: mass=Massformer-MLP, NEIMS=NEIMS encoder, MolMS=MolMS encoder.

2.3 Empirical study on learning rate

Next, we conducted comparisons of two learning rates across the MassBank [6], NPLIB1 [21], and MassSpecGym [22] datasets. The GNPS dataset [20] was excluded from these experiments due to its large size, which would require excessive computational time and resources. We use 2 learning rates, 10^{-4} and 10^{-3} .

The results, visualized in scatter plots in Fig. 2f comparing cosine similarity scores for each learning rate across various embedder-predictor-resolution combinations, reveal dataset-specific trends. In the MassBank and MassSpecGym datasets, learning rate 10^{-4} generally yields superior or comparable performance to 10^{-3} . Conversely, in the NPLIB1 dataset, the higher learning rate of 10^{-3} performs better. Notably, these trends are sometimes inconsistent across a diverse set of molecular embedders, predictor methods and spectral resolutions.

Supplementary Fig. A2 further shows that learning-rate effects are generally modest but dataset-dependent, with 10^{-4} tending to improve performance on MassBank and MassSpecGym while 10^{-3} is often favorable on NPLIB1; corresponding learning-rate sensitivity in CASMI16 spectrum-based retrieval is summarized in Supplementary Fig. A3.

This preference for lower learning rates in binned mass spectrum prediction can be attributed to several task-specific characteristics. Unlike drug-drug interaction or protein-protein interaction prediction which often involve classification, binned spectrum prediction requires modeling continuous intensity distributions across up to thousands of m/z bins where small parameter adjustments can significantly affect prediction quality [19]. Usually lower learning rates help mitigate the risk of overshooting minima in this complex landscape, allowing for more stable convergence [35].

To explain the divergent behavior in NPLIB1, where the higher learning rate of 10^{-3} outperforms 10^{-4} , we should consider the unique properties of these datasets. MassBank is a public repository of experimentally acquired mass spectra for small molecules, with high variability in spectral quality, noise, and fragmentation patterns due to diverse sources and instrumentation [6]. Similarly, MassSpecGym serves as a machine learning benchmark incorporating simulated and augmented spectra to highlight challenges like low-signal peaks, isotopic variations, and diverse structures, increasing complexity and gradient instability [22].

In contrast, the NPLIB1 dataset, derived from the Molecular Identification and Structure Tool integrated with the CANOPUS MS/MS computational method, features curated, high-quality spectra from natural products and metabolomics studies, with enhanced annotations for substructures and classes [21]. Its consistent, low-noise nature and predictable fragmentation rules create a smoother optimization landscape, allowing higher learning rates to enable faster convergence without overshooting.

The higher baseline cosine similarities in NPLIB1 indicate an easier prediction task, where aggressive updates can effectively leverage dataset regularities. This highlights the need to adapt hyperparameters to spectral diversity, noise, and annotation quality in mass spectrometry tasks [7].

2.4 Empirical study on insufficient training data

To examine the effects of limited training data on model performance in binned spectra predictions, we performed data ablation experiments using a scaffold split to subsample the training set, selecting 25% and 50% subsets to prevent data leakage while ensuring structural diversity. We trained models on 25%, 50%, and 100% of the training data, while maintaining full validation and test sets. This evaluates how embedder-predictor combinations scale under data constraints, mimicking real-world scenarios with sparse labeled data. All tests used the MassFormer predictor to focus on embedding impacts.

The results in Fig. 2b show trends in cosine similarity between embedders. Performance improves with more data, as expected, but gains vary. At 25% data, CNN achieves the best performance, followed by ESPF-MLP. Fingerprint-based methods such as Daylight-MLP and ChemBERTa also demonstrate strong results by effectively leveraging molecular priors. In contrast, GNN-type and Transformer-type models lag behind, with GCN performing particularly poorly due to the substantial data requirements for effective graph learning.

At 50%, GFv2 achieves the best performance, scaling well to 100% where it reaches peak performance. All types of GNN gain much from added data, closing gaps with fingerprints. This reflects fingerprints' efficiency via fixed features and domain knowledge, aiding low-data regimes, while GNNs require more samples to learn from raw graphs and risk overfitting. CNN excels in low data via local pattern capture, but plateaus versus GFv2.

Clear trade-offs emerge from these observations. GNNs excel in data-rich settings but underperform when data is sparse, while MLPs offer more balanced performance across data regimes. The diminishing returns in the past 50% suggest augmentation or hybrids for optimization. These insights highlight data-efficient architectures for the collection of costly mass spectrometry data.

2.5 Empirical study on pretrained models

To assess the impact of pretraining on molecular representation learning for mass spectrum prediction, we conducted experiments comparing a pretrained MoleBERT model against a randomly initialized version of the same architecture [38]. MoleBERT is a transformer-based model specifically designed for molecular data, featuring a multi-layer graph transformer architecture that processes molecular graphs as input. At its core, it employs graph attention mechanisms across multiple layers to capture node and edge features, incorporating positional encodings for atoms and bonds to preserve structural information. The model uses a BERT-like encoder with self-attention heads to generate contextual embeddings, followed by task-specific heads for pre-training objectives [39, 40].

In our setup, we integrated both the pretrained and randomly initialized MoleBERT as embedders within the FlexMS framework, paired with the MassFormer predictor for consistency with prior experiments.

Training and evaluation were performed on the MassSpecGym dataset with a bin resolution of 1, using cosine similarity, Jensen-Shannon divergence and coverage as performance metrics.

The results in Fig. 2c demonstrate a clear advantage for the pretrained MoleBERT across all evaluated scenarios. We find that in most cases, the pretrained model is generally better than the random model in all datasets and varying resolutions, particularly with MassFormer, while NEIMS and MolMS showed high performance regardless of initialization. This suggests that pretraining enhances generalization, especially in complex prediction tasks[41].

Furthermore, these findings underscore that pretrained chemical models like MoleBERT acquire foundational knowledge during self-supervised pretraining on large molecular datasets, which transfers effectively to diverse downstream applications. Even though the pretraining tasks—such as Masked Atoms Modeling for node-level prediction and context prediction—focus on structural understanding by masking discrete atom attributes and predicting surrounding graph contexts, this knowledge proves valuable in unrelated domains like binned spectra prediction in our setting. By learning robust representations of molecular graphs through these strategies, pretrained models reduce the need for task-specific data and improve performance in spectrum forecasting tasks, highlighting the versatility of chemical pretraining across computational chemistry workflows.

2.6 Empirical Study on Resolution Effects

In mass spectrometry, spectra are discretized into bins to facilitate computational prediction, with the resolution parameter defining bin width (e.g., 1 Da). Lower resolution values yield finer bins that preserve spectral detail but increase prediction complexity, while higher values produce coarser bins that aggregate peaks but may lose structural information.

We systematically evaluated molecular embedders integrated with three predictors across four datasets, measuring performance via cosine similarity and Jensen-Shannon divergence across resolutions from 1 Da to 10 Da. All models exhibited strong sensitivity to resolution changes, highlighting that optimal predictor selection depends heavily on specific binning strategies and dataset characteristics.

Results in Fig. 3 demonstrate a consistent positive correlation between coarser resolutions and prediction accuracy across all configurations. Critically, the improvement trajectory exhibits non-linear characteristics. The transition from res-1 to res-2 yields larger gains, showing the information aggregation. This pattern suggests that initial coarsening primarily eliminates critical noise and spurious peaks, while further aggregation offers less marginal benefit.

Model-specific sensitivity analysis reveals distinct architectural responses to resolution changes. Graph-based embedders exhibit stable and monotonic improvement curves, whereas sequence-based models and pre-trained language representations demonstrate more erratic trajectories, indicating differential robustness to spectral granularity variations.

2.7 Empirical study on Transfer Ability

To evaluate the transfer ability of our models on the MassSpecGym dataset, we conducted experiments focusing on domain adaptation across different ion types and instrument types. The MassSpecGym dataset comprises mass spectra where each spectrum is associated with an ion type of either $[M+H]^+$ or $[M+Na]^+$, and an instrument type of either QTOF or Orbitrap. We assessed transfer performance by training models on one subdomain and testing on the other. We trained on $[M+H]$ spectra and tested on $[M+Na]$ spectra, and vice versa. Similarly, we performed experiments training on QTOF spectra and testing on Orbitrap spectra, and vice versa.

The results, illustrated in Fig. 4a, reveal critical difference diagram and specific metric in model performance across these transfer scenarios. For ion types, models trained on MNa generally exhibit better generalization to MH than the reverse, as indicated by higher cosine similarity scores in the MNa-to-MH direction.

For instrument types, Orbitrap-trained models demonstrate a superior transfer to QTOF compared to that of QTOF-to-Orbitrap, with a lower Jensen-Shannon divergence in the former case. This indicates that models exposed to high-resolution Orbitrap data can better generalize to the lower-resolution QTOF domain.

These patterns can be explained by fundamental differences in fragmentation mechanisms and spectral characteristics documented in recent systematic studies of adduct-induced variability. For ion types, the asymmetric transfer performance reflects the distinct fragmentation pathways between $[M+Na]^+$ and $[M+H]^+$ species. Previous papers demonstrated that sodium-adducted ions exhibit markedly different fragmentation behavior, with a low spectral similarity to $[M+H]^+$ due to charge-remote fragmentation and coordination-based stabilization mechanisms that differ fundamentally from the charge-directed fragmentation of protonated species[42]. For instruments, Orbitrap’s superior mass resolution and accuracy provide a

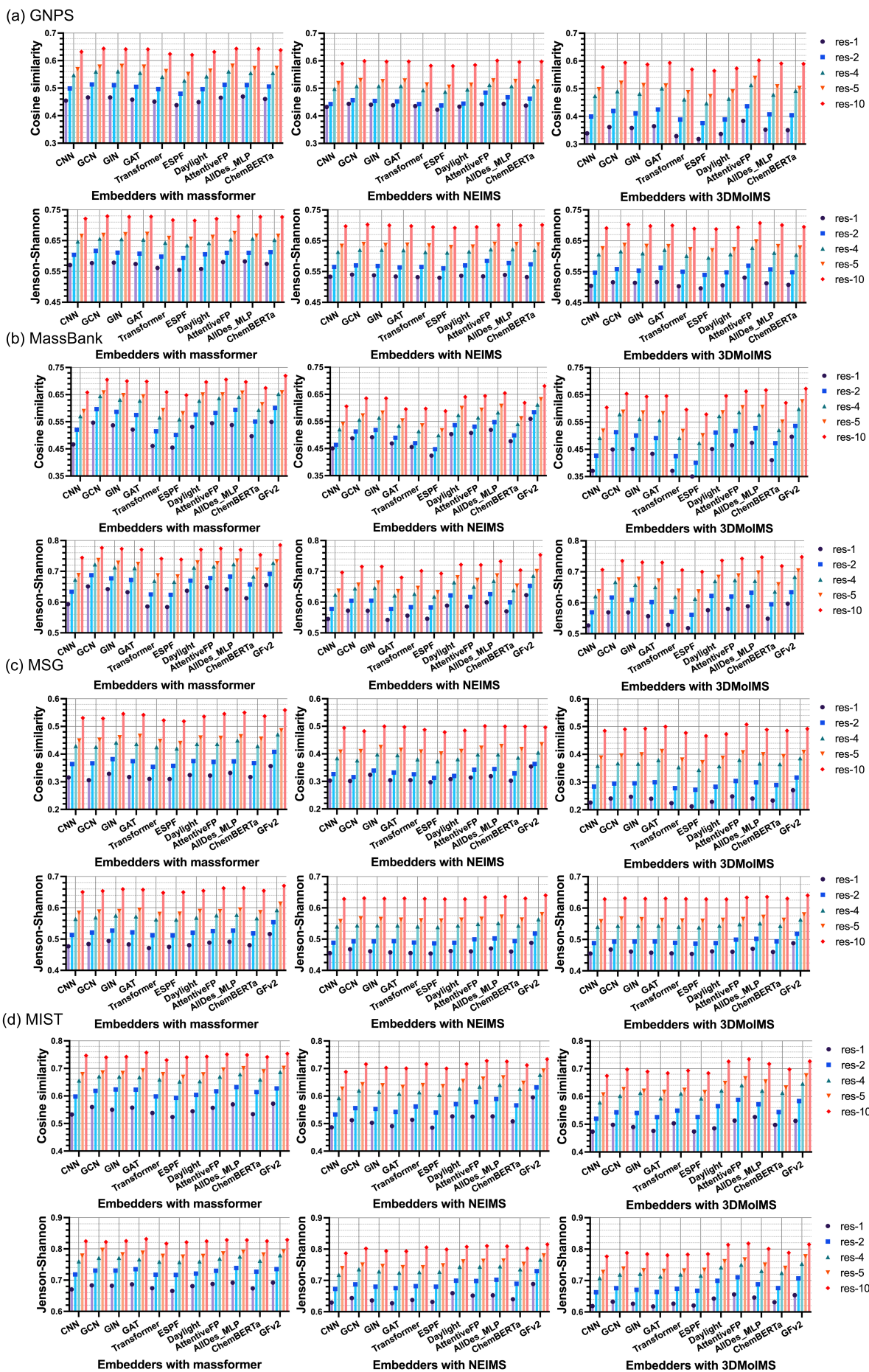


Fig. 3 Performance of different embedder-predictor combinations with different resolutions on GNPS dataset (random split), MassBank dataset (random split), MassSpecGym dataset and MIST dataset. Symbol "res-1", "res-2", "res-4", "res-5", "res-10" denote resolutions of 1, 2, 4, 5, and 10 Da respectively.

more detailed training signal, enabling models to downsample or adapt effectively to QTOF’s coarser resolution. In contrast, QTOF-trained models, constrained by lower precision, struggle to infer the fine-grained details required for Orbitrap predictions, leading to diminished performance in that direction[43].

Notably, the dataset exhibits significant imbalances: approximately 85% of the spectra are MH and 15% are MNa, while 75% are from Orbitrap and 25% from QTOF. The superior MNa-to-MH transfer is counterintuitive given the much smaller MNa training set, which challenges expectations that larger training domains should yield more robust models for transfer; this raises questions about underlying factors such as feature richness or domain similarity that may override sample size advantages. In contrast, the better Orbitrap-to-QTOF transfer aligns with the larger Orbitrap training set, supporting the role of data volume in facilitating generalization to smaller, lower-resolution domains.

These findings underscore the challenges in cross-domain transfer for mass spectrum prediction, emphasizing the need for domain-invariant representations or fine-tuning strategies to enhance model robustness across ion and instrument variations[44].

2.8 Empirical study on retrieval analysis

2.8.1 Task background

In addition to direct spectrum prediction evaluation, we assessed the practical utility of our binned prediction models through a retrieval task that simulates real-world mass spectrometry identification scenarios. The retrieval task represents a critical application where researchers attempt to identify unknown compounds by comparing their experimental mass spectra against databases of candidate molecules.

The retrieval evaluation follows a ranking-based approach similar to the CASMI (Critical Assessment of Small Molecule Identification) contest format [23], where for each query, the task involves an experimental mass spectrum of known molecule, a collection of candidate molecules that potentially match the query, and the objective of ranking all candidates so that the true molecule appears as high as possible in the ranked list.

2.8.2 Task Setting

We adapt the MassFormer evaluation framework to assess our models in a retrieval context, focusing exclusively on the CASMI 2016 and CASMI 2022 datasets to simulate compound identification challenges.

For CASMI 2016, the query set comprises Orbitrap spectra for 124 compounds after filtering for $[M+H]^+$ adducts and excluding charged species. Each spectrum is combined across normalized collision energies (NCE) of 20, 35, and 50. Candidate lists are derived from ChemSpider searches based on precursor mass similarity, yielding an average of 1,251 candidates per query after preprocessing. In Fig. 5b, we use the KDE plot to show the raw candidate number of 124 compounds. The plot shows most contest compound have about 1000 candidates, while only a few compound have more than 4000 candidates. The KDE peak is on the 500 candidates with a long-tail in raw KDE plot.

For CASMI 2022, the query set includes Orbitrap spectra for 228 compounds post-filtering for $[M+H]^+$ or $[M+Na]^+$ adducts and removal of unsupported elements. We use this subset because most datasets only have $[M+H]^+$ or $[M+Na]^+$ data and other ionized data are out of this distribution. Massformer method generates candidate by sampling from PubChem within a 10 ppm mass tolerance of the query precursor, capped at 10,000 per query. After filtering unsupported elements, multimolecular compounds, and deduplicating stereoisomers, this results in an average of 4,849 candidates per spectrum. This setup emphasizes scenarios with minimal prior knowledge beyond approximate mass and adduct type. In Fig. 5b, we also showed the KDE plot of CASMI22 dataset. The KDE plot for the CASMI 2022 dataset reveals a skewed distribution with a prominent peak near the upper limit of 10,000 candidates, indicating that a substantial number of compounds in contrast to the more moderate candidate counts observed in CASMI 2016.

In the retrieval process, we begin by organizing the candidate molecules according to their associated query molecules. For each query spectrum, which includes detailed metadata such as absolute or normalized collision energies, instrument type, ionization mode, precursor m/z , and the list of observed peaks, we associate these experimental conditions with every candidate molecule in the corresponding set. Each candidate is then linked to its structural representation in the form of a SMILES string, and the ground-truth peak list from the query spectrum is paired with all candidates for subsequent comparison.

Following this preparation, we filter out any candidates lacking valid structural information to ensure data integrity. The resulting dataset is then transformed into a suitable format for model input, with any incomplete entries removed to maintain consistency. Using our trained model, we generate predicted spectra for all candidates under the exact experimental conditions of the query. These predictions, along with the groundtruth spectra, are used to compute cosine similarities for each candidate-query pair.

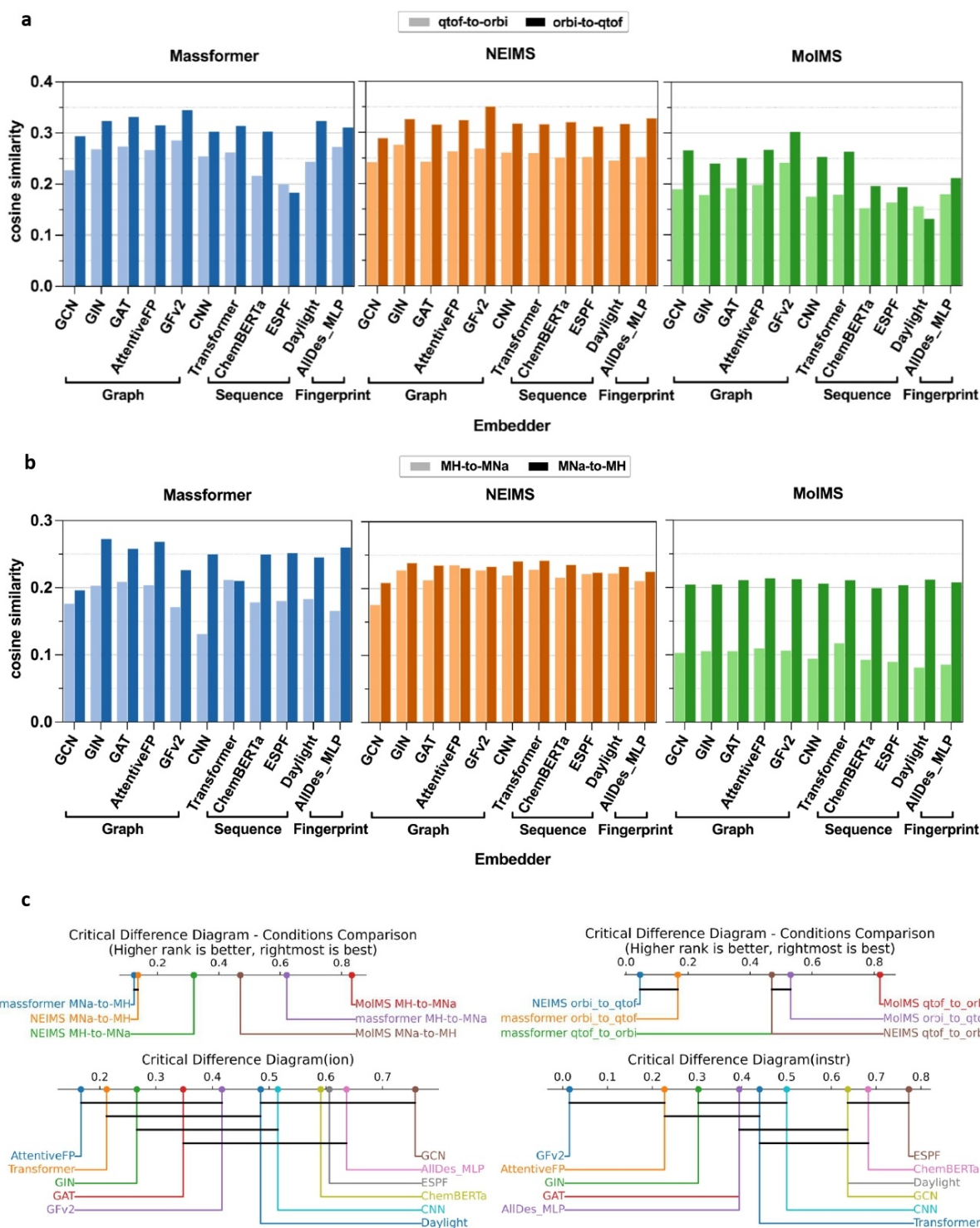


Fig. 4 (a)(b) Detailed performance comparison of domain transfer. (a) Ionization mode transfer. (b) Instrument type transfer. (c) The critical difference diagram of different transfer case and embedders. Left is ion-transfer case and right is instrument-transfer case.

Performance is quantified using several metrics averaged across queries: raw rank, normalized rank, top-1,5,10 and top-1%,5%,10%. These metrics evaluate both absolute and relative ranking effectiveness, highlighting the model's ability to prioritize the correct structure amid large candidate pools.

2.8.3 Benchmark Result

On the basis of the retrieval results table, several important patterns emerge that provide insights into the performance characteristics of different molecular embedders for mass spectrometry identification tasks.

From Fig. 5a, GFv2 demonstrates exceptional and consistent performance across all resolution settings, achieving the best normalized ranks of 0.086 and 0.151 in CASMI16 and CASMI22 respectively. This represents the top performance among all embedders tested. Such consistency suggests that GFv2’s molecular representations are robust and well-suited for spectrum-based molecular identification. As shown in Fig. 5c, the cumulative performance and kernel density estimate of the GFv2-MassFormerMLP embedder-predictor architecture reveal that the top 25% of compounds achieve a normalized rank of less than 1%, the top 50% less than 3%, and the top 75% less than 18% in CASMI22. These results highlight the accuracy of the Massformer architecture.

Most embedders display varying degrees of sensitivity to increasing spectral resolution, often showing notable performance degradation as normalized ranks rise from 1 Da to 10 Da. Traditional fingerprint-based approaches and graph neural networks are particularly vulnerable, exhibiting sharp declines as resolution increases. In contrast, embedders such as GFv2 and MLPs prove more robust, maintaining relatively stable performance across resolutions. An important note is that modest increases in resolution result in minimal performance drops for many methods while offering significant savings in training resources, making them a practical choice for balancing computational efficiency and retrieval accuracy in mass spectrometry tasks.

About different architectures, graph neural network methods generally perform better than other fingerprint approaches in Fig. 5d. Except GFv2, GCN achieves the best performance among GNN methods at lower resolutions but degrades more at higher resolutions. All-descriptor-based MLP also performs well, suggesting that carefully selected molecular features can be effective for retrieval tasks. Notably, while GCN performs poorly in prediction benchmarks probably due to challenges in generating exact spectral output, it excels in retrieval scenarios, suggesting that its architecture is particularly adept at embedding and comparing molecular similarities for ranking purposes rather than precise spectral simulation.

These benchmark results underscore the profound influence of embedder selection on retrieval performance in mass spectrometry identification, where top performers such as GFv2 can deliver normalized ranks that are superior to those of average methods and far exceed the poorest, leading to more efficient and accurate candidate retrieval. Given the varying sensitivity to spectral resolution across embedders with many showing marked declines in effectiveness at higher resolutions, researchers should carefully align their model choices with the target resolution to optimize outcomes, as this can significantly affect consistency in real-world applications.

3 Methods

3.1 Datasets

To comprehensively evaluate the robustness and generalizability of our framework, we have curated a diverse suite of datasets. This multi-faceted collection was selected to represent the various scenarios encountered in metabolic research, allowing us to systematically assess model performance across different data scales, qualities, and downstream applications. The suite includes a standardized machine learning benchmark (MassSpecGym), large-scale public spectral libraries (GNPS and MassBank), a high-quality curated collection (NPLIB1) and a real-world identification contest (CASMI). The key characteristics of these datasets are summarized in Table 4.

3.1.1 MassSpecGym Dataset

MassSpecGym [22] serves as a foundational platform for evaluating model performance in a controlled environment. It is the largest publicly available collection of high-quality, labeled tandem mass spectra, comprising 231,000 spectra from 29,000 unique molecules. The dataset was specifically designed for machine learning applications, featuring highly standardized metadata (e.g., ionization adducts, instrument types). A key advantage of MassSpecGym is its rigorous data-splitting procedure based on molecular edit distance, which is designed to prevent data leakage and provide a robust assessment of a model’s ability to generalize to novel chemical structures.

3.1.2 GNPS Dataset

To test model performance under realistic, large-scale conditions, we incorporate the Global Natural Products Social Molecular Networking (GNPS) library[20]. As a massive, open-access, and crowdsourced ecosystem, GNPS contains over 322,000 spectra from more than 16,000 molecules, characterized by significant heterogeneity from diverse instruments, laboratories, and experimental protocols. The inherent noise and variability within GNPS make it an excellent testbed for evaluating the robustness and scalability of prediction models when faced with the complexities of real-world, community-contributed data.

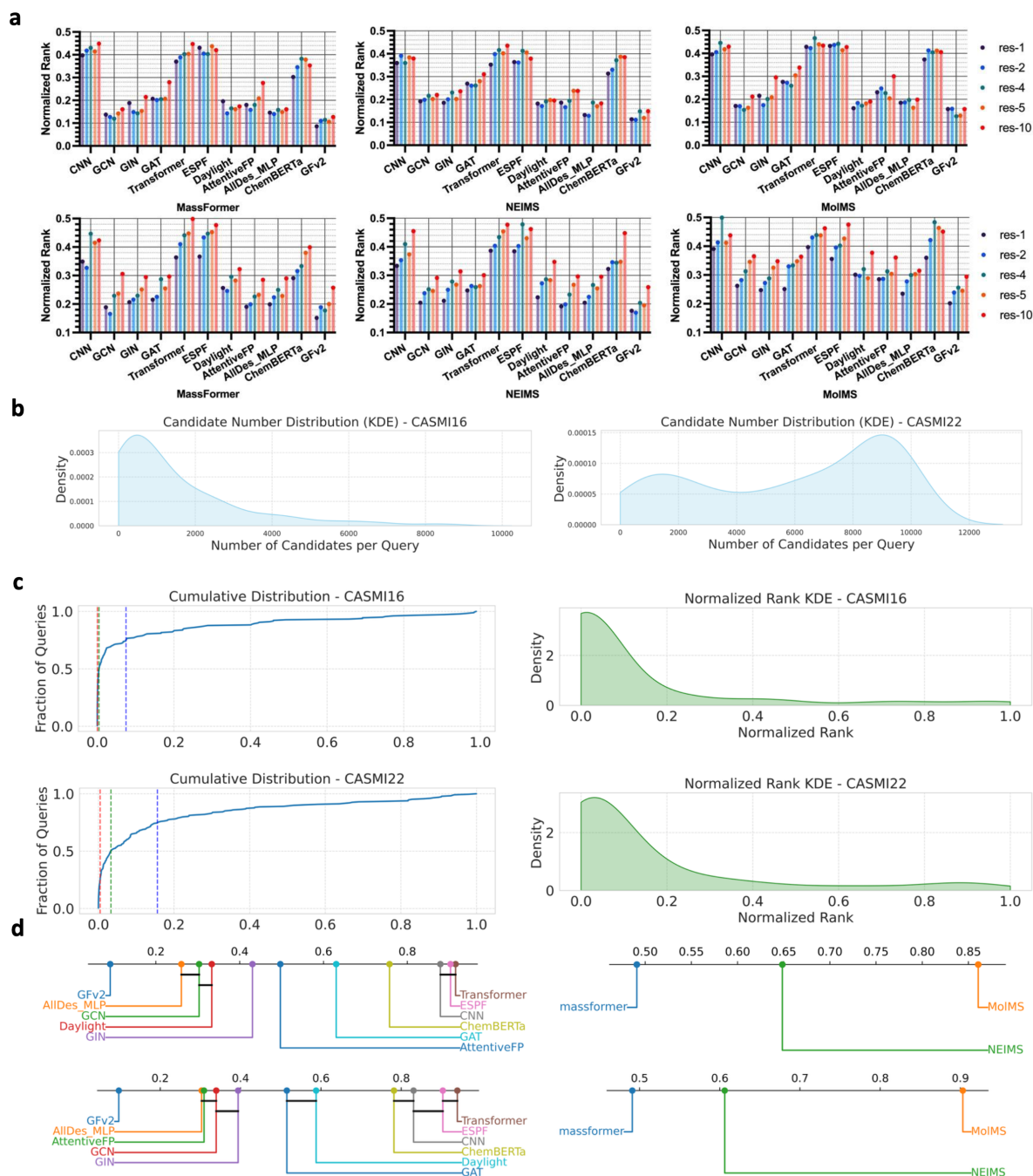


Fig. 5 (a) The normalized rank of different predictors and embedders on CASMI16 and CASMI22 contest. Different lines represent different resolutions, and res-1, res-2, res-4, res-5, res-10 denote resolutions of 1, 2, 4, 5, and 10 Da respectively. (b) The KDE plot of CASMI compound's candidate number distribution. We showed on both CASMI16 and CASMI22 contest. (c) The cumulative distribution and KDE plot of the normalized-rank performance on GFv2-MassFormerMLP combinations. (d) The Critical Difference Diagram of different embedders and predictors on CASMI16 and CASMI22 contest. We compared the performance on normalized rank, so lower value means better rank.

3.1.3 MassBank Dataset

As one of the first public repositories for mass spectra, MassBank[6] is another cornerstone for our evaluation. It provides a rich, open-source library of over 62,000 spectra from more than 4,000 small chemical compounds, many of which are high-resolution. MassBank's established role in the metabolomics community makes it an essential dataset for ensuring our framework's compatibility and performance on foundational, widely-used public data resources, complementing the scale of GNPS with its historical depth and focus on reference-quality spectra.

Dataset	Approx. Size	Key Characteristic
MassSpecGym	231k spectra 29k molecules	Standardized ML benchmark with clean metadata and generalization-aware data splits. It serves as a modern baseline for evaluating deep learning models across diverse chemical spaces.
GNPS	>322k spectra >16k molecules	Large-scale, crowdsourced library with significant real-world noise and heterogeneity.
MassBank	>62k spectra >4k molecules	The first public repository, offering a rich source of high-resolution spectra. It enforces strict record validation and open data standards to ensure high reliability for metabolomics identification.
NPLIB1	~8k spectra/~7k molecules	Curated natural products collection with balanced chemical classes and high-quality spectra. It serves as a critical testbed for evaluating model performance on biologically relevant chemical spaces.
CASMI16/22	Challenge-based datasets	Real-world compound identification task, requiring ranking of candidate structures.

Table 4 Overview of Datasets Used for Benchmarking

3.1.4 NPLIB1 Dataset

For more targeted analyses where data quality and balance are critical, we employ the NPLIB1 benchmark dataset which was used in the development of MIST and CANOPUS[21]. This dataset consists of approximately 8,000 high-quality spectra from 7,000 unique natural products. Its defining feature is the careful curation process that ensures an even distribution across chemical classes. This controlled environment is ideal for isolating the effects of specific factors, such as hyperparameters, without the confounding biases present in larger, more heterogeneous datasets.

3.1.5 CASMI contest

Beyond evaluating spectral prediction accuracy, we assess the practical utility of our framework on a critical downstream task: compound identification. For this, we utilize challenges from the Critical Assessment of Small Molecule Identification (CASMI) contest[23], an ongoing initiative aimed at advancing methods for identifying small molecules from mass spectrometry data. To simulate real-world scenarios, CASMI periodically releases high-resolution mass spectrometry datasets, such as the CASMI 2016 test set which comprised 230 chemicals. The core task in these challenges is to correctly identify the true molecular structure for a given query spectrum from a provided list of candidates. This simulates a common workflow in untargeted metabolomics and directly measures a model’s real-world applicability. By evaluating our models’ performance in this competitive setting, we can gauge their potential to accelerate scientific discovery.

3.2 Data Split Evaluation and Model Comparison Framework

3.2.1 Molecule splits setting

In dataset partitioning for cheminformatics applications, random split assigns individual molecules to training, validation, or test sets purely stochastically, which may inadvertently place structurally analogous entities across different sets. In contrast, scaffold split first identifies the core molecular scaffold of each compound and then allocates all compounds sharing a common scaffold to the same dataset partition[27]. The latter approach aims to provide a more stringent evaluation of model ability to generalize on chemical space.

For the GNPS and MassBank datasets, we implemented both random and scaffold-based splitting methodologies to partition the data as 80%:10%:10% for training and evaluation. In contrast, the MassSpecGym and NPLIB1 datasets were utilized with their intrinsically provided data splits, precluding the need for external partitioning strategies for these specific benchmarks.

3.2.2 Kolmogorov-Smirnov Test and Murcko Metric on molecule splits

Let each molecule x be represented by a binary Morgan fingerprint $\mathbf{f}(x) \in \{0, 1\}^d$ on ECFP radius r and bit-length d . For two molecules x, y , with $a = \|\mathbf{f}(x)\|_1$, $b = \|\mathbf{f}(y)\|_1$, and $c = \mathbf{f}(x)^\top \mathbf{f}(y)$, the Tanimoto similarity is $T(x, y) = \frac{c}{a+b-c} \in [0, 1]$.

Given splits Train, Val and test, we form similarity pairs $Pair$. On dataset with large unique molecules, uniform random sampling is taken when the Cartesian product is large.

$$\begin{aligned} Pair_{Train-Train} &= \{T(x_i, x_j) : x_i, x_j \in Train, i \neq j\} \\ Pair_{Train-Val} &= \{T(x_i, y_j) : x_i \in Train, y_j \in Val\} \\ Pair_{Train-Test} &= \{T(x_i, x_j) : x_i \in Train, y_j \in Test\} \end{aligned} \quad (1)$$

For any sample $\{s_i\}_{i=1}^n$ of similarities, its empirical CDF is defined as $\hat{F}_n(t) = \frac{1}{n} \sum_{i=1}^n \mathbf{1}\{s_i \leq t\}$.

To test whether Train-Val distributions and Train-Test distributions differ (e.g., $Pair_{Train-Train}$ vs. $Pair_{Train-Val}$), the two-sample Kolmogorov-Smirnov (KS) statistic is defined as $D_{n,m}$.

$$D_{n,m} = \sup_{t \in \mathbb{R}} |\hat{F}_n(t) - \hat{G}_m(t)|, \quad (2)$$

\hat{F}_n and \hat{G}_m are the empirical CDFs of the two samples of sizes n and m . Under the null hypothesis H_0 that both samples are drawn from the same continuous distribution, the null distribution of $D_{n,m}$ depends on the effective sample size

$$n_{\text{eff}} = \frac{nm}{n+m}, \quad Z = D_{n,m} \sqrt{n_{\text{eff}}}. \quad (3)$$

The corresponding p -value has the Kolmogorov tail with the large- Z asymptotic approximation. We reject H_0 at level α if $p < \alpha$.

$$\begin{aligned} p &= \mathbb{P}(D_{n,m} \sqrt{n_{\text{eff}}} \geq Z) = 2 \sum_{k=1}^{\infty} (-1)^{k-1} e^{-2k^2 Z^2} \text{ (for normal } Z) \\ p &\approx 2e^{-2Z^2} \text{ (for large } Z). \end{aligned} \quad (4)$$

For scaffold overlap using Murcko scaffolds $\sigma(\cdot)$, let $\Sigma(\mathcal{A}) = \{\sigma(x) : x \in \mathcal{A}\}$. Two common normalizations are

$$\text{overlap}_{\text{test in train}} = \frac{|\Sigma(\mathcal{A}) \cap \Sigma(\mathcal{B})|}{|\Sigma(\mathcal{B})|}, \quad \text{Jaccard overlap} = \frac{|\Sigma(\mathcal{A}) \cap \Sigma(\mathcal{B})|}{|\Sigma(\mathcal{A}) \cup \Sigma(\mathcal{B})|}. \quad (5)$$

Scaffold splits target near-zero overlap, while random splits typically yield moderate overlap.

3.2.3 Spectral Entropy Analysis

To complement the structural similarity analysis from the input perspective, we employ spectral entropy besides cosine similarity to assess distributional shifts from the output (spectral) perspective. Previous work shows that entropy has more information in library matching compared with cosine similarity and provided more information [30]. For a spectrum with n peaks of intensities $\{I_i\}_{i=1}^n$, the spectral entropy is defined as:

$$H = - \sum_{i=1}^n p_i \ln(p_i), \quad \text{where } p_i = \frac{I_i}{\sum_{j=1}^n I_j} \quad (6)$$

Here, p_i represents the normalized intensity of the i -th peak, and H is measured in nats. We compute spectral entropy for all spectra in each dataset split and apply the two-sample KS test to compare entropy distributions between training and validation/test sets.

3.2.4 Critical Difference Diagram with Wilcoxon-Holm Method

To evaluate the relative performance of k models across N datasets, we employ the Critical Difference Diagram based on average ranks. The average rank \bar{R}_j for model C_j is calculated as:

$$\bar{R}_j = \frac{1}{N} \sum_{i=1}^N r_{i,j}, \quad (7)$$

where $r_{i,j}$ is the rank of C_j on dataset i . Statistical significance is determined using a Friedman test followed by a post-hoc Wilcoxon signed-rank test. To control the Family-Wise Error Rate (FWER) across m pairwise comparisons, we apply the Holm-Bonferroni correction. For ordered p -values $p_1 \leq \dots \leq p_m$, a hypothesis H_i is rejected if:

$$p_i \leq \frac{\alpha}{m - i + 1}, \quad (8)$$

where $\alpha = 0.05$. In the CD diagram, classifiers are positioned by \bar{R}_j , and a thick horizontal line connects groups of classifiers where the null hypothesis is not rejected, indicating no statistically significant difference in performance.

3.3 MetaData Embedding

In our model architecture, metadata associated with mass spectra is absolute collision energy (ACE), normalized collision energy (NCE), instrument type, precursor type, ion mode, and precursor $\mathbf{m/z}$. They are embedded into a compact numerical representation to facilitate integration with the neural network. This embedding process is performed during the transformation of the data set and is crucial for conditioning the model on the experimental parameters.

The embedding begins by handling missing values and normalizing continuous features. For ACE and NCE, binary indicators are created to flag missing values. The non-missing values are then standardized by subtracting the mean and dividing by the standard deviation with missing values filled as -1 post-normalization. Categorical features, including instrument type, precursor type and ion mode, are converted to one-hot encoding. If the number of unique categories in the current dataset differs from a predefined count, the one-hot vectors are zeroed out to maintain dimensionality consistency. Precursor $\mathbf{m/z}$ is binned into integer values and treated as a discrete feature.

The final metadata embedding is formed by concatenating these processed components. This vector is then passed as input to the model’s metadata encoder, enabling the integration of spectral context into the learning process. This approach ensures robustness to missing data and provides a standardized input format for downstream tasks in the FlexMS framework.

3.4 Featurizer architectures

3.4.1 Traditional Featurizers

We implemented a suite of traditional featurizer methods that convert molecular structures into fixed-length vector representations, primarily using fingerprints and physicochemical descriptors as inputs for downstream machine learning models. These approaches leverage RDKit and related libraries to encode structural and property-based features[45].

Morgan fingerprints, which generate bit vectors through circular hashing of atomic environments with a specified radius and bit length, capturing substructural patterns[46]. **MACCS keys** provide a predefined set of 166 structural fragments for binary encoding[47]. **Physicochemical descriptors** compute molecular properties such as exact molecular weight, logP, hydrogen bond donors and acceptors, rotatable bonds, atom counts, molar refractivity, topological polar surface area, formal charge, and ring counts. Atom pair fingerprints encode pairs of atoms and their topological distances in a hashed vector. **Extended-reduced Graph(ErG) fingerprints** represent simplified molecular graphs for similarity comparisons[48]. **Daylight fingerprints** use path-based hashing to produce binary vectors of 2048 bits[49]. PubChem fingerprints generate 881-bit vectors based on predefined substructures[50]. A concatenated descriptor featurizer combines Morgan, Morgan counts, MACCS, physicochemical, atom pair, and ErG features into a unified representation.

3.4.2 Sequence-Based Molecular Representation Featurizers

Inspired by sequence processing in natural language models, we introduced featurizers that treat SMILES strings as sequential data, enabling embedding generation through encoding and transformer-based methods. One-hot encoding transforms SMILES characters into categorical vectors, padding or truncating to a maximum sequence length with a predefined alphabet of 58 symbols, including atoms, bonds, and special tokens.

Explainable Substructure Partition fingerprint (ESPF) featurizers employ byte-pair encoding (BPE) on SMILES strings using a ChEMBL-derived vocabulary, producing tokenized sequences with optional masking and a maximum length for transformer compatibility[51]. **ChemBERTa** is employed as a model-based featurizer as well [9]. Instead of deriving representations through hand-crafted encoding schemes, the featurization directly utilizes the output embeddings generated by the pretrained masked language model applied to tokenized SMILES sequences. Fixed-dimensional molecular representations are subsequently obtained by post-processing the results of token embeddings.

3.4.3 Graph-Based Molecular Representation Featurizers

To exploit the inherent graph structure of molecules, we incorporated graph neural network-compatible featurizers using DGL and RDKit, converting SMILES into graph objects with node and edge features[45, 52].

Canonical featurizers employ atom and bond encoders for basic graph construction, including atomic numbers, chirality, hybridization, and bond types, with self-loops and optional virtual nodes for padding to a node count. AttentiveFP featurizers extend this with attention-based atom and bond features, capturing local environments through multi-head mechanisms[53]. 3D featurizers generate complete graphs from single conformers, embedding 3D coordinates and distances using Alchemy-inspired node and edge features after conformer optimization via UFF force fields. A simplified molecular graph featurizer converts RDKit molecules into PyTorch Geometric data objects, encoding atomic numbers, chirality, bond types, and directions in a sparse adjacency format suitable for graph neural networks[54].

3.5 Model Architectures

FlexMS adopts a modular design philosophy, decoupling the mass spectrum prediction pipeline into two distinct components: the **Molecule Embedding Model** (Embedder) and the **Spectrum Predictor** (Predictor). This modularity allows for the systematic benchmarking of arbitrary combinations of molecular encoders and prediction heads [35].

3.5.1 Molecule Embedding Models

The role of the embedder is to map the specific molecular features defined in Section 3.4 into a fixed-dimensional latent vector, h_{mol} , which encapsulates the structural and chemical information of the molecule. FlexMS integrates a wide range of widely-used architectures:

- **MLP-based Embedders:** For vector-based fingerprints (e.g., Morgan, MACCS), we employ Multi-Layer Perceptrons (MLPs) with residual connections to map high-dimensional sparse vectors into dense latent representations.
- **Sequence-based Embedders:** For SMILES sequences, we utilize 1D-CNNs to capture local patterns from one-hot encodings [8]. Additionally, we incorporate Transformer-based encoders, including a standard encoder adapted from DeepPurpose [55] and the pre-trained *ChemBERTa* model [9], to capture long-range dependencies through self-attention mechanisms.
- **Graph Neural Networks (GNNs):** For graph inputs, we implement standard message-passing architectures including Graph Convolutional Networks (GCN) [37], Graph Attention Networks (GAT) [32], and Graph Isomorphism Networks (GIN) [31]. Furthermore, to evaluate the impact of advanced architectures, we include *AttentiveFP* [53] and *Graphormer (GFv2)*, the latter of which utilizes the sophisticated spatial encodings described in Section 3.4.3.

3.5.2 Spectrum Predictors

The predictor serves as the decoder, taking the concatenated vector of the molecular embedding h_{mol} and the metadata embedding h_{meta} (encoding collision energy and precursor type) as input to generate the final binned mass spectrum. FlexMS adapts three distinct predictor architectures from state-of-the-art studies to represent different modeling paradigms:

- **MassFormer Predictor:** Adapted from the MassFormer architecture [15], this predictor represents a high-capacity MLP design. It features a **bidirectional prediction mechanism**, which explicitly models two processes: the forward generation of fragments and the reverse neutral loss from the precursor ion. A learnable gating mechanism dynamically weighs the contribution of these two streams, allowing the model to better capture peaks in both low and high m/z regions.
- **NEIMS Predictor:** Adapted from the NEIMS framework [19], this predictor represents an efficiency-focused design. It utilizes a streamlined MLP architecture that prioritizes inference speed. While simpler than MassFormer, it also incorporates bidirectional logic to handle the physical constraints of fragmentation, providing a strong baseline for computational efficiency.
- **MolMS Predictor:** Adapted from the 3DMolMS framework [34], this predictor represents a deep residual learning approach. It employs an encoder-decoder structure where the decoding block is composed of multiple fully connected layers with Residual Blocks. This architecture allows for deeper networks without vanishing gradient issues, theoretically enabling the modeling of more complex non-linear relationships between molecular structure and spectral intensity.

3.6 Evaluation Metrics on binned spectra prediction

In mass spectrometry, evaluating the quality of predicted or generated spectra often involves comparing them to experimentally derived reference spectra. This comparison is quantified using various similarity metrics, each capturing different aspects of spectral resemblance. Key metrics include Cosine Similarity, Jensen-Shannon Similarity, and Spectral Coverage. These metrics provide complementary information about spectral similarity. Raw spectral data are preprocessed by log1p intensity transformation and normalization, which help to reduce the dominance of very intense peaks and emphasize the overall pattern.

Cosine similarity

Cosine Similarity is a widely adopted metric that measures the cosine angle between predicted and groundtruth spectral vectors. It reflects the similarity of peak patterns and their relative intensities. The similarity is the dot product of two L-2 normalized vectors.

$$\begin{aligned} \mathbf{y}_{pred}^* &= \frac{\mathbf{y}_{pred}}{\|\mathbf{y}_{pred}\|_2} \\ \mathbf{y}_{true}^* &= \frac{\mathbf{y}_{true}}{\|\mathbf{y}_{true}\|_2} \\ \text{cos}(\mathbf{y}_{pred}^*, \mathbf{y}_{true}^*) &= \mathbf{y}_{pred}^* \cdot \mathbf{y}_{true}^* \end{aligned} \tag{9}$$

Jensen-Shannon similarity

Jensen-Shannon Similarity provides a measure of similarity between two probability distributions[56]. In our context, both predicted and groundtruth mass spectra are treated as probability distributions by normalizing their intensities. Therefore, we derived Jensen-Shannon Similarity from the Jensen-Shannon divergence, which is a symmetrized and smoothed version of the Kullback-Leibler divergence[57].

$$\begin{aligned} \text{JS}_{\text{div}} &= \frac{1}{2} \cdot (D_{KL}(y_{pred}||M) + D_{KL}(y_{true}||M)) \\ M &= (y_{pred} + y_{true})/2 \\ \text{JS}_{\text{sim}} &= 1 - \text{JS}_{\text{div}} \end{aligned} \tag{10}$$

Spectral Coverage

Spectral coverage is a binary metric that evaluates the extent to which significant peaks in the groundtruth spectrum are present in the predicted spectrum, focusing on peak presence rather than intensity matching. After binarizing both spectra using a predefined threshold τ , spectral coverage is calculated as the ratio of peaks present in both binarized spectra to the total number of peaks in the binarized groundtruth spectrum.

This metric is particularly valuable for assessing whether prediction methods successfully identify key fragment ions, as a high coverage score indicates that most significant peaks are captured regardless of exact intensity values, which is crucial in mass spectrometry applications where the presence of specific fragment ions is more important than their precise abundance ratios for molecular identification and structural elucidation.

$$\begin{aligned} y_{gt_bin}[i] &= \begin{cases} 1 & \text{if } y_{true}[i] \geq \tau \\ 0 & \text{if } y_{true}[i] < \tau \end{cases} \\ y_{pred_bin}[i] &= \begin{cases} 1 & \text{if } y_{pred}[i] \geq \tau \\ 0 & \text{if } y_{pred}[i] < \tau \end{cases} \\ \text{Coverage} &= \frac{\sum(y_{gt_bin} \cdot y_{pred_bin})}{\sum y_{gt_bin}} \end{aligned} \tag{11}$$

3.7 Metric on Spectrum-based Molecule Retrieval

In spectrum-based molecule retrieval tasks, such as those in the CASMI contest, the goal is to rank a set of candidate molecules based on the similarity between their predicted spectra and the query spectrum of a target molecule. The evaluation involves comparing predicted spectra (generated from candidate molecules) against the ground-truth spectrum of the query molecule. Similarity is typically computed using cosine similarity on the spectral vectors. Candidates are then ranked by this similarity score, and performance is assessed by how highly the true query molecule ranks among the candidates. Key metrics include absolute rank, normalized rank, and top-K / top-K

Absolute Rank and Normalized Rank

Rank measures the position of the true query molecule in the sorted list of candidates, where candidates are ordered by descending cosine similarity between their predicted spectra and the ground-truth query spectrum. Here, candidate_i denotes the i -th candidate in this sorted list (with indexing starting from 0). A lower rank (ideally 0) indicates better performance. Normalized Rank scales the rank by the size of the retrieval group containing the query molecule, providing a relative measure between 0 and 1.

$$\begin{aligned} \text{Rank}_{\text{query-mol}} &= \arg \min_i (\text{candidate}_i = \text{query-mol}) \\ \text{Normalized_Rank}_{\text{query-mol}} &= \frac{\text{Rank}_{\text{query-mol}}}{\text{Total_Candidates}_{\text{query-mol}}} \end{aligned} \tag{12}$$

These metrics are computed for each query and averaged across all queries to evaluate overall model performance. Cosine similarity is used as the ranking criterion, applied element-wise to the predicted and ground-truth spectral vectors after appropriate preprocessing.

Top-K Accuracy

Top-K Accuracy assesses whether the true query molecule appears within the top K positions in the ranked list. It is a binary indicator (1 if true, 0 otherwise) for each query, and the mean across all queries gives the proportion of successful top-K retrievals. Common values include Top-1 (exact match at the top), Top-5, and Top-10. Here, Rank refers to the absolute rank of the query molecule as defined previously, and N is the number of queries.

$$\begin{aligned} \text{Top-K}_{\text{query-mol}} &= 1 \text{ if } \text{Rank}_{\text{query-mol}} < K, 0 \text{ otherwise} \\ \text{Mean Top-K} &= \frac{1}{|Q|} \sum_{\text{query-mol} \in Q} \text{Top-K}_{\text{query-mol}} \end{aligned} \tag{13}$$

where N is the number of queries. This metric emphasizes the model’s ability to prioritize the correct molecule in the highest ranks.

Top-K% Accuracy

Top-K% Accuracy is similar to Top-K but uses a percentage-based threshold on the Normalized Rank. It checks if the true molecule ranks within the top K% of candidates (e.g., $\text{Normalized_Rank} < 0.01$ for Top-1%). This is particularly useful for varying candidate set sizes across queries, providing a normalized view of retrieval success. Here, Normalized Rank is as defined previously, and N is the number of queries.

$$\begin{aligned} \text{Top-K}\%_{\text{query-mol}} &= 1 \text{ if } \text{Normalized_Rank}_{\text{query-mol}} < \frac{K}{100}, 0 \text{ otherwise} \\ \text{Mean Top-K}\% &= \frac{1}{N} \sum_{q=1}^N \text{Top-K}\%_q \end{aligned} \tag{14}$$

Common thresholds include Top-1%, Top-5%, and Top-10%. Like Top-K, the mean is reported as the final metric.

These retrieval metrics collectively evaluate the effectiveness of spectrum-based ranking. Rank and Normalized Rank provide direct measures of positioning, while Top-K and Top-K% offer hit-rate perspectives at different granularities. They are computed after grouping candidates by query, inferring predictions, and sorting by cosine similarity, ensuring comprehensive assessment in tasks with diverse candidate pools.

3.8 Model training

We tested the influence of many hyperparameters in predicting binned spectra, and we fixed the other hyperparameters.

For CNN, we use 3 1d-Conv blocks with channels 32, 64, 96 and kernel size 4, and output dimension is 256. For GAT, we use 3 DGL GAT blocks with ReLU and hidden dimension 64, and the output dimension is 64. For GCN, we use 1 DGL GCN blocks with ReLU and 3 hidden dimensions 64, and the output dimension is 256. For GIN, we used 4 DGL GINConv layers, each with batch normalization and ReLU activation. Each GINConv layer contains a 2-layer MLP with the hidden dimension set to 64. and the hidden dimension and output dimension is 64. For the Transformer, we used 8 transformer layers with 8

attention heads with hidden size 512, and its output embedding dimension of 128. For AttentiveFP, we used 2 AttentiveFPGNN layers with node feature size 39 and edge feature size 11, and the output dimension is 64. For ESPF, Daylight and All-descriptors MLPs, we use same MLP architecture with different input sizes, and the MLP model has 3 hidden size 1024, 256, 64 and ReLU-activation layers.

4 Discussion

The introduction of FlexMS is an advance in the adoption of a standard flexible benchmarking framework for deep-learning based mass spectrum prediction, which has been a long-standing challenge in metabolomics with sectioned dataset heterogeneity and the absence of evidence-based benchmarks. Our findings offer in-depth analysis on the behavior of different molecular embedders and predictors as well as hyperparameters on multiple cases. FlexMS points out this way both strengths and limitations from current methods, providing valuable practical information for new model design without overfitting.

A methodological contribution of this work is the dual-perspective validation of dataset partitioning strategies. While Tanimoto similarity analysis assesses structural diversity at the molecular input level, our spectral entropy analysis [30] examines distributional shifts at the spectral output level. The consistency between these two independent analyses—with scaffold splits exhibiting 4–7 times larger KS statistics than random splits in both perspectives—provides strong evidence that scaffold-based partitioning genuinely creates out-of-distribution generalization challenges.

One key point highlighted in our experiments is the significantly better performance of graph-based embedders, with pretrained GFv2 showing robust advantages over other models across multiple datasets, predictors and resolutions for both direct spectrum prediction and retrieval [16]. However, this comes at a cost, as GFv2’s larger model size and higher computational demands may limit its use in resource-constrained environments, suggesting a pragmatic trade-off: while GFv2 is the gold standard for accuracy-critical tasks, simpler architectures like GIN or GAT represent the ‘sweet spot’ for high-throughput screening, offering competitive performance with orders of magnitude lower latency.

We find dataset-specific optima in our learning rates, lower learning rates leading to better performance on noisier heterogeneous datasets such as MassBank or MassSpecGym, likely requiring smaller gradient adjustments in complex optimization landscapes. On the other hand, higher learning rates were used for the curated NPLIB1 less-noisy dataset leading to an accelerated convergence. This points the importance of hyperparameters with respect to data characteristics such as the quality of spectra or variability in the number of peaks.

In the same vein, data ablation experiments show the robustness of fingerprint-based approaches in low-data regimes, where they use predefined molecular priors to reduce overfitting while GNNs need access to more training instances for effectively capturing their inductive biases. These are important considerations in the context of real-world metabolomics studies where high quality annotated spectra are often limited and suggest appealing strategies such as data augmentation. This explicitly demonstrates the trade-off between inductive bias and data availability: fingerprint-based methods provide strong chemical priors that stabilize learning in low-data regimes, whereas GNNs act as data-hungry universal approximators that require scale to surpass these heuristic baselines [7, 36].

The pretraining effect, which is observed through the improvement of MoleBERT pretrained over random initialization, justifies the transfer learning in chemistry [9, 38, 41]. Pretrained models empower to learn basic structural knowledge from massive SMILES or graph corpora and generalize well on spectrum prediction to alleviate data requirement on downstream tasks. This is true in particular for more complex predictors like MassFormer, where pretraining improves generalisation.

As for spectral resolution, the increasing performance observed toward coarser bins indicates a trade-off between detail preservation and noise reduction; finer resolutions increase the difficulty of prediction by requiring detailed intensity modeling over more bins, while coarser resolutions form clusters of more signals into an individual bin, making predictions easier but possibly losing interpretability for some applications with high-resolution fragmentation analysis.

The poor generalization observed in transfer learning experiments reveals intriguing asymmetries, with more favorable performance when transferring from $[M+Na]^+$ to $[M+H]^+$ ion types and from Orbitrap to QTOF instruments, even in the presence of dataset class imbalances that might suggest otherwise. This could stem from the richer fragmentation patterns in $[M+Na]^+$ spectra or the higher fidelity of Orbitrap data [42, 43]. These findings highlight the challenges of domain shift in MS/MS prediction, where factors such as adduct-specific behaviors and instrument variations can lead to performance degradation, underscoring the need to develop domain-invariant representations or employ adversarial training to improve cross-domain robustness [44].

In search benchmark akin to a CASMI challenge set, GFv2 maintains its superiority with robust performance on moderate-size candidate bases. The preference for moderate resolution increases provides a

practical way of trading off computational efficiency and high product quality, and the scaling performance solely in ranking tasks suggests that GCN is appropriate for similarity-based problems. On the whole, these results serve to validate FlexMS ability to standardize evaluations demonstrating that advanced GNNs do well while a simple fingerprint still holds its own in a tightly constrained environment.

Despite these advances, limitations persist. At present, FlexMS is limited to binned prediction, which could ignore possibly modellable detail from fragmentation or formula-based methods. This discretization strategy effectively transforms the stochastic fragmentation process into a tractable multi-label regression problem, avoiding the complexity of variable-length output generation and enabling standardized, metric-driven benchmarking. Public data sources can introduce bias towards compound classes, and exclusion of proprietary data limits generalizability. Computational requirements of state-of-the-art models such as GFv2 may limit scalability.

In the future, we aim to extend FlexMS for further prediction paradigms and other types of datasets, and we will consider real-time factors such as collision energy changes. FlexMS offers the community an open-source platform for sharing developments, which in turn will help accelerate the 'filling in' of gaps within spectral libraries and accordingly increase capacity to discover small molecules in drug discovery and metabolic.

5 Code and Data availability

The data for all figures and tables are provided in the Figshare. The code is open-source at <https://doi.org/10.6084/m9.figshare.31144669> and data is open-source at <https://doi.org/10.6084/m9.figshare.31144573>.

6 Acknowledgement

This research is supported by National Natural Science Foundation of China Project (No. 623B2086), TeleAI of China Telecom, Ant Group, CIPS-SMP research funding for Large Language Models and Tencent.

References

- [1] Aebersold, R., Mann, M.: Mass-spectrometric exploration of proteome structure and function. *Nature* **537**(7620), 347–355 (2016)
- [2] De Hoffmann, E., Stroobant, V.: *Mass Spectrometry: Principles and Applications*. John Wiley & Sons, Chichester, England (2007)
- [3] Kind, T., Tsugawa, H., Cajka, T., Ma, Y., Lai, Z., Mehta, S.S., Wohlgemuth, G., Barupal, D.K., Showalter, M.R., Arita, M., *et al.*: Identification of small molecules using accurate mass ms/ms search. *Mass spectrometry reviews* **37**(4), 513–532 (2018)
- [4] Dührkop, K., Fleischauer, M., Ludwig, M., Aksenov, A.A., Melnik, A.V., Meusel, M., Dorrestein, P.C., Rousu, J., Böcker, S.: Sirius 4: a rapid tool for turning tandem mass spectra into metabolite structure information. *Nature methods* **16**(4), 299–302 (2019)
- [5] Wishart, D.S., Feunang, Y.D., Marcu, A., Guo, A.C., Liang, K., Vázquez-Fresno, R., Sajed, T., Johnson, D., Li, C., Karu, N., *et al.*: Hmdb 4.0: the human metabolome database for 2018. *Nucleic acids research* **46**(D1), 608–617 (2018)
- [6] Horai, H., Arita, M., Kanaya, S., Nihei, Y., Ikeda, T., Suwa, K., Ojima, Y., Tanaka, K., Tanaka, S., Aoshima, K., *et al.*: Massbank: a public repository for sharing mass spectral data for life sciences. *Journal of mass spectrometry* **45**(7), 703–714 (2010)
- [7] Yang, K., Swanson, K., Jin, W., Coley, C., Eiden, P., Gao, H., Guzman-Perez, A., Hopper, T., Kelley, B., Mathea, M., *et al.*: Analyzing learned molecular representations for property prediction. *Journal of chemical information and modeling* **59**(8), 3370–3388 (2019)
- [8] Hirohara, M., Saito, Y., Koda, Y., Sato, K., Sakakibara, Y.: Convolutional neural network based on smiles representation of compounds for detecting chemical motif. *BMC bioinformatics* **19**(Suppl 19), 526 (2018)
- [9] Chithrananda, S., Grand, G., Ramsundar, B.: Chemberta: large-scale self-supervised pretraining for molecular property prediction. *arXiv preprint arXiv:2010.09885* (2020)
- [10] Fabian, B., Edlich, T., Gaspar, H., Segler, M., Meyers, J., Fiscato, M., Ahmed, M.: Molecular representation learning with language models and domain-relevant auxiliary tasks. *arXiv preprint arXiv:2011.13230* (2020)
- [11] Goldman, S., Li, J., Coley, C.W.: Generating molecular fragmentation graphs with autoregressive neural networks. *Analytical Chemistry* **96**(8), 3419–3428 (2024)
- [12] Goldman, S., Bradshaw, J., Xin, J., Coley, C.: Prefix-tree decoding for predicting mass spectra from molecules. *Advances in Neural Information Processing Systems* **36**, 48548–48572 (2023)
- [13] Standards, N.I., Technology: NIST 20 Mass Spectral Library (NIST/EPA/NIH). NIST/EPA/NIH Mass Spectral Library and NIST Tandem Mass Spectral Library (2020)
- [14] Ridder, L., Hooft, J.J.J., Verhoeven, S.: Automatic compound annotation from mass spectrometry data using magma. *Mass Spectrometry* **3**(Special Issue 2), 0033–0033 (2014)
- [15] Young, A., Röst, H., Wang, B.: Tandem mass spectrum prediction for small molecules using graph transformers. *Nature Machine Intelligence* **6**(4), 404–416 (2024)
- [16] Ying, C., Cai, T., Luo, S., Zheng, S., Ke, G., He, D., Shen, Y., Liu, T.-Y.: Do transformers really perform badly for graph representation? *Advances in Neural Information Processing Systems* **34**, 28877–28888 (2021)
- [17] Allen, F., Greiner, R., Wishart, D.: Competitive fragmentation modeling of esi-ms/ms spectra for putative metabolite identification. *Metabolomics* **11**(1), 98–110 (2015)
- [18] Ruttkies, C., Schymanski, E.L., Wolf, S., Hollender, J., Neumann, S.: Metfrag relaunched: incorporating strategies beyond in silico fragmentation. *Journal of cheminformatics* **8**(1), 3 (2016)

- [19] Wei, J.N., Belanger, D., Adams, R.P., Sculley, D.: Rapid prediction of electron-ionization mass spectrometry using neural networks. *ACS central science* **5**(4), 700–708 (2019)
- [20] Wang, M., Carver, J.J., Phelan, V.V., Sanchez, L.M., Garg, N., Peng, Y., Nguyen, D.D., Watrous, J., Kaponov, C.A., Luzzatto-Knaan, T., *et al.*: Sharing and community curation of mass spectrometry data with global natural products social molecular networking. *Nature biotechnology* **34**(8), 828–837 (2016)
- [21] Dührkop, K., Nothias, L.-F., Fleischauer, M., Reher, R., Ludwig, M., Hoffmann, M.A., Petras, D., Gerwick, W.H., Rousu, J., Dorrestein, P.C., *et al.*: Systematic classification of unknown metabolites using high-resolution fragmentation mass spectra. *Nature biotechnology* **39**(4), 462–471 (2021)
- [22] Bushuiev, R., Bushuiev, A., Jonge, N., Young, A., Kretschmer, F., Samusevich, R., Heirman, J., Wang, F., Zhang, L., Dührkop, K., *et al.*: Massspecgym: A benchmark for the discovery and identification of molecules. *Advances in Neural Information Processing Systems* **37**, 110010–110027 (2024)
- [23] Schymanski, E.L., Ruttkies, C., Krauss, M., Brouard, C., Kind, T., Dührkop, K., Allen, F., Vaniya, A., Verdegem, D., Böcker, S., *et al.*: Critical assessment of small molecule identification 2016: automated methods. *Journal of cheminformatics* **9**(1), 22 (2017)
- [24] Mason, J.S., Hermsmeider, M.A.: Diversity assessment. *Current opinion in chemical biology* **3**(3), 342–349 (1999)
- [25] Rogers, D., Hahn, M.: Extended-connectivity fingerprints. *Journal of chemical information and modeling* **50**(5), 742–754 (2010)
- [26] Bajusz, D., Rácz, A., Héberger, K.: Why is tanimoto index an appropriate choice for fingerprint-based similarity calculations? *Journal of cheminformatics* **7**(1), 20 (2015)
- [27] Wu, Z., Ramsundar, B., Feinberg, E.N., Gomes, J., Geniesse, C., Pappu, A.S., Leswing, K., Pande, V.: Moleculenet: a benchmark for molecular machine learning. *Chemical science* **9**(2), 513–530 (2018)
- [28] Berger, V.W., Zhou, Y.: Kolmogorov–smirnov test: Overview. *Wiley statsref: Statistics reference online* (2014)
- [29] Schuffenhauer, A., Ertl, P., Roggo, S., Wetzler, S., Koch, M.A., Waldmann, H.: The scaffold tree- visualization of the scaffold universe by hierarchical scaffold classification. *Journal of chemical information and modeling* **47**(1), 47–58 (2007)
- [30] Li, Y., Kind, T., Folz, J., Vaniya, A., Mehta, S.S., Fiehn, O.: Spectral entropy outperforms ms/ms dot product similarity for small-molecule compound identification. *Nature Methods* **18**(12), 1524–1531 (2021)
- [31] Xu, K., Hu, W., Leskovec, J., Jegelka, S.: How powerful are graph neural networks? *arXiv preprint arXiv:1810.00826* (2018)
- [32] Veličković, P., Cucurull, G., Casanova, A., Romero, A., Lio, P., Bengio, Y.: Graph attention networks. *arXiv preprint arXiv:1710.10903* (2017)
- [33] Demšar, J.: Statistical comparisons of classifiers over multiple data sets. *Journal of Machine learning research* **7**(Jan), 1–30 (2006)
- [34] Hong, Y., Li, S., Welch, C.J., Tichy, S., Ye, Y., Tang, H.: 3dmolms: prediction of tandem mass spectra from 3d molecular conformations. *Bioinformatics* **39**(6), 354 (2023)
- [35] Liebal, U.W., Phan, A.N., Sudhakar, M., Raman, K., Blank, L.M.: Machine learning applications for mass spectrometry-based metabolomics. *Metabolites* **10**(6), 243 (2020)
- [36] Wu, Z., Pan, S., Chen, F., Long, G., Zhang, C., Yu, P.S.: A comprehensive survey on graph neural networks. *IEEE transactions on neural networks and learning systems* **32**(1), 4–24 (2020)
- [37] Kipf, T.: Semi-supervised classification with graph convolutional networks. *arXiv preprint arXiv:1609.02907* (2016)

- [38] Xia, J., Zhao, C., Hu, B., Gao, Z., Tan, C., Liu, Y., Li, S., Li, S.Z.: Mole-bert: Rethinking pre-training graph neural networks for molecules (2023)
- [39] Devlin, J., Chang, M.-W., Lee, K., Toutanova, K.: Bert: Pre-training of deep bidirectional transformers for language understanding. In: Proceedings of the 2019 Conference of the North American Chapter of the Association for Computational Linguistics: Human Language Technologies, Volume 1 (long and Short Papers), pp. 4171–4186 (2019)
- [40] Vaswani, A., Shazeer, N., Parmar, N., Uszkoreit, J., Jones, L., Gomez, A.N., Kaiser, L., Polosukhin, I.: Attention is all you need. *Advances in neural information processing systems* **30** (2017)
- [41] Rong, Y., Bian, Y., Xu, T., Xie, W., Wei, Y., Huang, W., Huang, J.: Self-supervised graph transformer on large-scale molecular data. *Advances in neural information processing systems* **33**, 12559–12571 (2020)
- [42] Liu, B., Tang, Z., Huan, T.: Adduct-induced variability in tandem mass spectrometry. *Analytical Chemistry* **97**(31), 17058–17066 (2025)
- [43] Deschamps, E., Calabrese, V., Schmitz, I., Hubert-Roux, M., Castagnos, D., Afonso, C.: Advances in ultra-high-resolution mass spectrometry for pharmaceutical analysis. *Molecules* **28**(5), 2061 (2023)
- [44] Zhuang, F., Qi, Z., Duan, K., Xi, D., Zhu, Y., Zhu, H., Xiong, H., He, Q.: A comprehensive survey on transfer learning. *Proceedings of the IEEE* **109**(1), 43–76 (2020)
- [45] Bento, A.P., Hersey, A., Félix, E., Landrum, G., Gaulton, A., Atkinson, F., Bellis, L.J., De Veij, M., Leach, A.R.: An open source chemical structure curation pipeline using rdkit. *Journal of Cheminformatics* **12**(1), 51 (2020)
- [46] Morgan, H.L.: The generation of a unique machine description for chemical structures—a technique developed at chemical abstracts service. *Journal of chemical documentation* **5**(2), 107–113 (1965)
- [47] Durant, J.L., Leland, B.A., Henry, D.R., Nourse, J.G.: Reoptimization of mdl keys for use in drug discovery. *Journal of chemical information and computer sciences* **42**(6), 1273–1280 (2002)
- [48] Stiefl, N., Watson, I.A., Baumann, K., Zaliani, A.: Erg: 2d pharmacophore descriptions for scaffold hopping. *Journal of chemical information and modeling* **46**(1), 208–220 (2006)
- [49] James, C.A.: Daylight theory manual. <http://www.daylight.com/dayhtml/doc/theory/theory.toc.html> (2004)
- [50] Helal, K.Y., Maciejewski, M., Gregori-Puigjane, E., Glick, M., Wassermann, A.M.: Public domain hts fingerprints: design and evaluation of compound bioactivity profiles from pubchem’s bioassay repository. *Journal of chemical information and modeling* **56**(2), 390–398 (2016)
- [51] Huang, K., Xiao, C., Glass, L., Sun, J.: Explainable substructure partition fingerprint for protein, drug, and more. In: *NeurIPS Learning Meaningful Representation of Life Workshop* (2019)
- [52] Wang, M., Zheng, D., Ye, Z., Gan, Q., Li, M., Song, X., Zhou, J., Ma, C., Yu, L., Gai, Y., et al.: Deep graph library: A graph-centric, highly-performant package for graph neural networks. *arXiv preprint arXiv:1909.01315* (2019)
- [53] Xiong, Z., Wang, D., Liu, X., Zhong, F., Wan, X., Li, X., Li, Z., Luo, X., Chen, K., Jiang, H., et al.: Pushing the boundaries of molecular representation for drug discovery with the graph attention mechanism. *Journal of medicinal chemistry* **63**(16), 8749–8760 (2019)
- [54] Fey, M., Lenssen, J.E.: Fast graph representation learning with pytorch geometric. *arXiv preprint arXiv:1903.02428* (2019)
- [55] Huang, K., Fu, T., Glass, L.M., Zitnik, M., Xiao, C., Sun, J.: Deeppurpose: a deep learning library for drug–target interaction prediction. *Bioinformatics* **36**(22-23), 5545–5547 (2020)
- [56] Menéndez, M.L., Pardo, J.A., Pardo, L., Pardo, M.d.C.: The jensen-shannon divergence. *Journal of the Franklin Institute* **334**(2), 307–318 (1997)

- [57] Kullback, S., Leibler, R.A.: On information and sufficiency. *The annals of mathematical statistics* **22**(1), 79–86 (1951)

Appendix A Supplementary

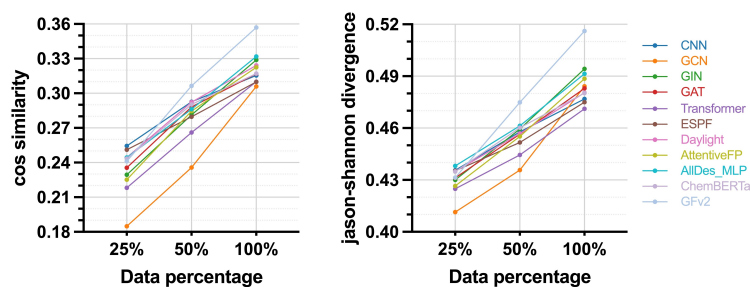


Fig. A1 Supplementary Figure 1. Performance evaluation (cosine similarity and JS divergence) of various embedders on the MassSpecGym dataset in data-limited regimes. Training sets were reduced to half and quarter sizes with constant validation and test sets, using a fixed MassFormer-MLP predictor.

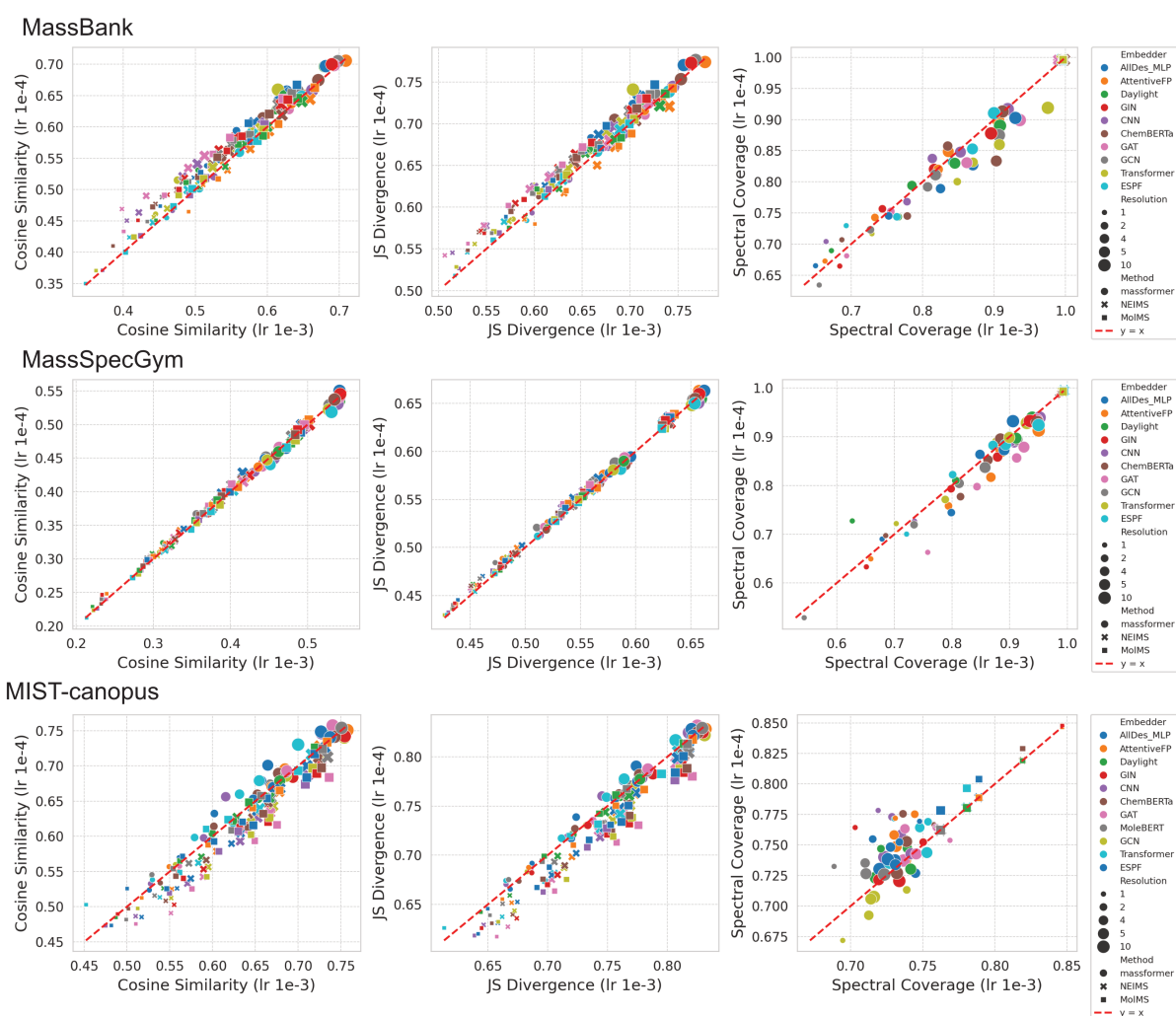


Fig. A2 Supplementary Figure 2. Cosine similarity, JS divergence, and coverage across different learning rates and conditions. The analysis evaluates all combinations of embedders, predictors, and resolutions.

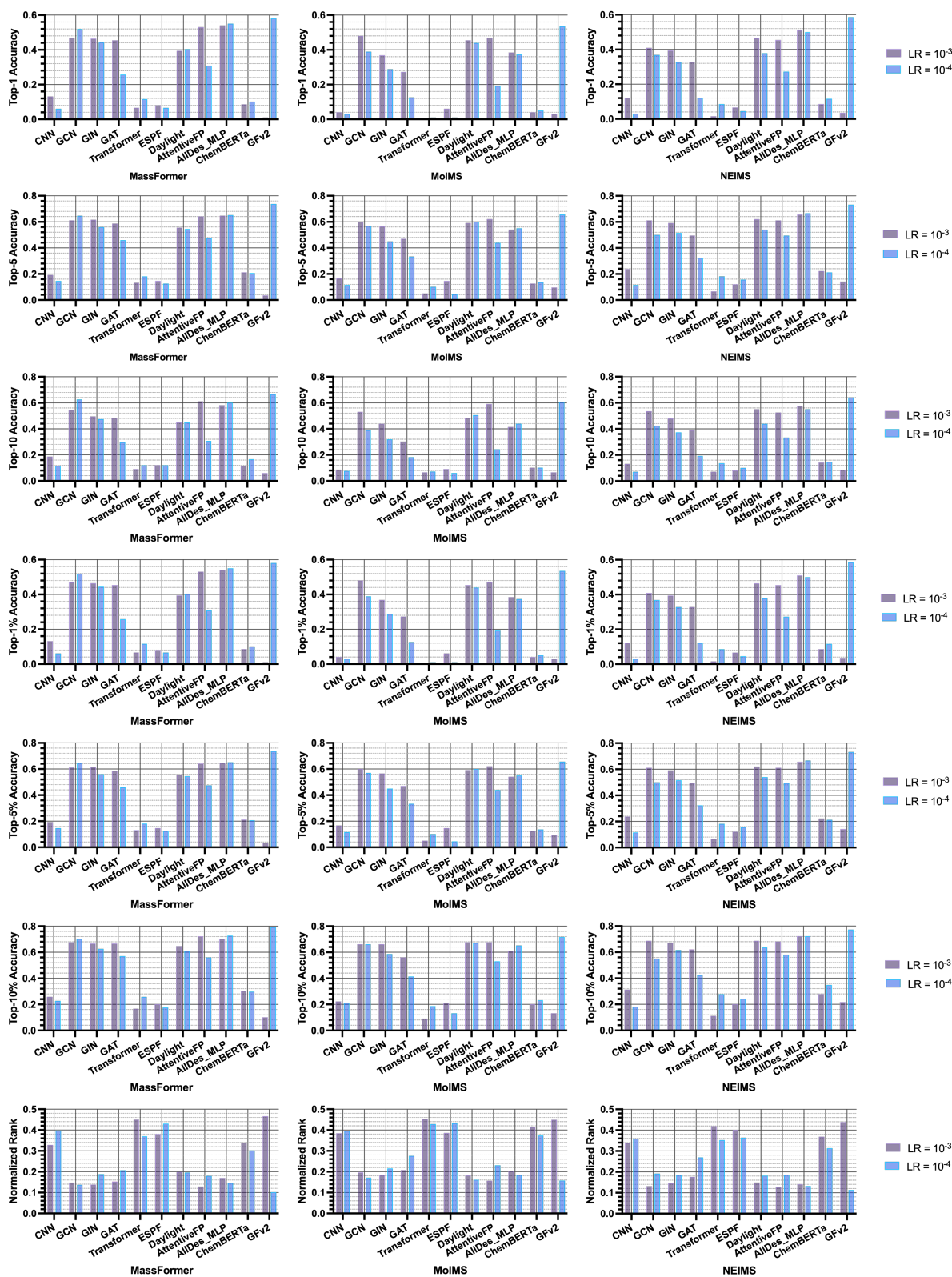


Fig. A3 Supplementary Figure 3. Retrieval performance metrics on the CASMI16 dataset across different learning rates. Various metrics were evaluated for this task.

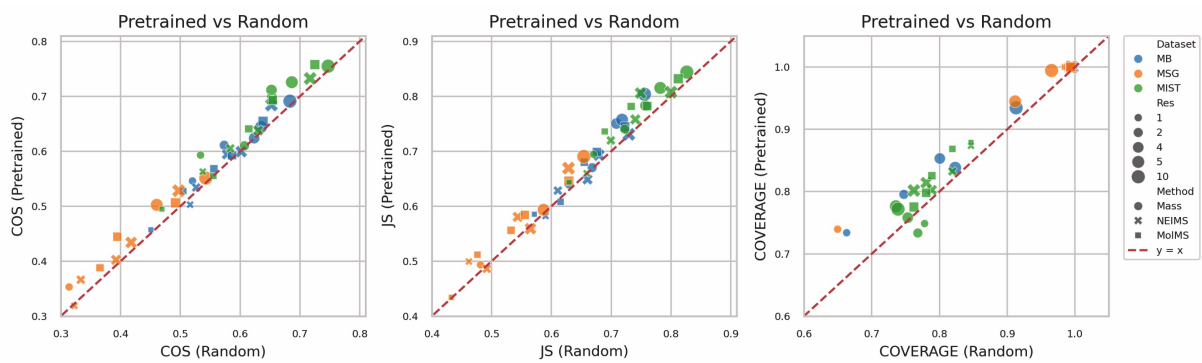


Fig. A4 Supplementary Figure 4. Performance metrics between pretrained MoleBERT and random-initialized MoleBERT. Various metrics and datasets(MassBank, MIST-canopus and MassSpecGym) are evaluated for this task.